Appendix O.1

Battery Energy Storage System
Preliminary Fire Risk Assessment and Heat Flux Analysis

Starlight Solar
Major Use Permit PDS2022-MUP-22-010
Battery Energy Storage System
Preliminary NFPA 551 Preliminary Fire Risk Assessment and Heat Flux Analysis

20250320-SLS-AW0764-BESS-FRA-R2

Issued: 23 July 2025

AHJ Revision Notice: This Preliminary NFPA 551 Fire Risk Assessment (FRA) and Heat Flux Analysis is provided as a "Land Use Permit" approval analysis to support the initial permitting of the Starlight Solar Energy Storage Project in San Diego County California. This NFPA 551 FRA and Heat Flux Analysis was created using the best available OEM information and addresses the majority of the liquid cooled GridSolv Quantum design failure modes that could result in fire, shock, explosion, or injury to personnel. This document shall not be used for final compliance determination.

This Preliminary FRA was also completed based on the presumption of the eventual provision of the completion and provision of Project Standard and Emergency Operating Procedures, updated Wartsila GridSolv Quantum Design Documentation, and the associated updating of the Nationally Recognized Testing Laboratory UL9540 Certificate and Report.

Upon issuance of the Project Standard and Emergency Operating Procedures, this Preliminary FRA shall be updated to reflect the installed configuration as required by IFC Section 1207.1.4.

Prepared for:

Empire II, LLC
12302 Exposition Blvd.
Los Angeles, CA 90068

Issued by:

Hiller
2120 Capital Drive
Wilmington NC 28405

Disclaimer

The Hiller Companies provides Energy Storage System Engineering Consulting services based on the information available at the time of consultation and the details provided by the client. All engineering products, reports, and services are subject to the following:

1. **Energy Storage Systems are Hazardous**: Energy Storage Systems, regardless of the technology, are hazardous and can result in unanticipated safety events including fire, shock, explosion, equipment damage, and injury to personnel.
2. **No Warranties**: The Hiller Companies makes no warranties, express or implied, regarding the accuracy, completeness, or suitability of the consulting services provided. All recommendations and advice are given in good faith and based on professional knowledge, international industry consensus standards, engineering judgement, and based on the limited information provided by the client at the time of consultation.
3. **Limitations of Liability**: The Hiller Companies shall not be held liable for any direct, indirect, incidental, consequential, or any other type of facility or equipment damage, or injury to personnel arising out of the use or reliance on the consulting services provided. This includes, but is not limited to, damages for loss of profits, business interruption, or loss of information.
4. **Risk Acknowledgment**: The client acknowledges that engineering projects may involve inherent risks, including but not limited to, technical failures, design errors, and unforeseen issues. The Hiller Companies is not responsible for any risks that may arise during the execution of engineering projects. All engineering products are based upon the efficacy of the information provided by the client.
5. **Client Responsibility**: The client is responsible for: providing factual data, analyses, drawings and other engineering related documents for contracted services and the verification & validation of any final recommendations, decisions and implementation of any information provided by The Hiller Companies. The client acknowledges that any actions taken based on the consulting services are at their own risk.
6. **Third-Party Products and Services**: The Hiller Companies does not take responsibility for the performance, reliability, or safety of any third-party products or services recommended or referred to during the consultation process. Hiller is not responsible for the associated system design or performance for work done by others that includes cascading failures of interdependent systems. The client is advised to conduct their own due diligence when selecting and using such products and services.
7. **Regulatory Compliance**: The Hiller Companies provides consulting services with the understanding that the client is responsible for ensuring that their engineering projects comply with all applicable laws, regulations, and standards. The Hiller Companies is not liable for any non-compliance or legal issues arising from the client's engineering projects.

Table of Contents

Revision History

Revision	Date	Description
0	24 April 2025	Released for Client Dissemination
1	20 May 2025	Declaration of Basis of Design
2	23 July 2025	Redefinition of the intent of the document as preliminary at the client. Title page and appropriate verbiage changed as directed by client.

Executive Summary

This Preliminary NFPA 551 Fire Risk Assessment (FRA) and Heat Flux Analysis was conducted to evaluate the hazards and risks associated with a theoretical UL9540 compliant energy storage system for the Empire II LLC Starlight Project. The Empire II LLC Starlight Project is an eight-parcel project located in San Diego County, southeast of Manzanita CA in proximity of 32.66016162785173, -116.28052568720432.

This FRA and Heat Flux Analysis addresses a potential bounding design basis fire event per the requirements of California Fire Code (CFC) §1207.1.4 and NFPA 855:2023, Section 4.4.2.1.(1) [1, 2]. This FRA evaluates the fire risk associated with the thermal runaway of an original equipment manufacturer (OEM) agnostic Lithium-Iron Phosphate (LFP) based energy storage system (ESS). The information presented in this FRA assumes an unlikely failure event where all safety critical controls fail to operate upon demand to create the bounding fire event. In the event of the design-basis fire, this FRA also establishes the maximum, theoretical, momentary design-basis accident heat flux that could be realized by an adjacent BESS or San Diego County First Responders.

This FRA also assumes the requisite CFC §1207.1.5 Large Scale Fire Test (LSFT) has been conducted, and compliance is assumed based on the observations of the Fire Protection Engineer of Record for the Starlight Project.

The methodologies used in this Fire Risk Assessment are based on internationally recognized OSHA Process Safety Management (PSM) [3] for the reliance on recognized and generally accepted good engineering practices [4]. These engineering practices utilize numerous international consensus standards and market sector testing data to ensure the efficacy of the quantitative and qualitative analyses. Specifically, the Society of Fire Protection Engineers (SFPE) Engineering Guide, *Fire Risk Assessments* was used to frame the Fire Risk Assessment format to be compliant with the requirements of the National Fire Protection Association (NFPA) Standard 551, *Guide for the Evaluation of Fire Risk Assessments*. Where necessary to compute the radiant heat at the adjacent Energy Storage Units and structure adjacencies, the *SFPE Handbook of Fire Protection Engineering* and NFPA *Fire Protection Handbook* as well as other peer-reviewed research and publications were relied upon to establish the -technical basis for the applicable computations. The application of each standard and peer reviewed document is referenced throughout this report.

This FRA is a fundamental element of the integrated documents necessary for construction submittal in accordance with NFPA 855 and the California Fire Code (CFC). The results of this FRA are intended to address the specific Fault Conditions of the CFC § 1207.1.4 resulting in a design-basis fire and provided sufficient information leading to the Authority Having Jurisdiction Approval.

The enabling scenario for the Starlight Project assumes an unmitigated fire where all non-certified Safety components fail to operate to create the maximum theoretical (design-basis) fire and the resultant heat flux.

While today's energy storage safety codes and standards acknowledge cascading thermal runaway as a risk, they stop short of prohibiting it, and fail to address the risk of non-flaming heat transfer to neighboring cells, modules, and racks [5]. Therefore, to address the associated risk, the magnitude of the fire risk is quantified and presented herein.

Based on our research, and the subsequent numerical analysis, we have determined there is not an increased probability that with unmitigated thermal and electrical abuse an exothermic reaction and thermal runaway could occur for the Starlight stationary energy storage system based on the ESS design [6].

This FRA assumes a bounding design-basis accident scenario where all uncertified Safety protection (SIL) measures are assumed to fail or fail to perform engineered function or operate upon demand. To establish the maximum theoretical design basis fire event, this analysis assumes module to module propagation event though the UL9540A Module Level Test of the OEM objectively demonstrates there was no module-to-module propagation observed [7-9]. Based on this scenario, the calculated maximum theoretical momentary peak heat release rate of a fully engaged *ESS* energy segment due to the ignition of flammable gases and continued consumption of the lithium-ion fuel in a single rack is 16.4 MW as function of the percentage of lithium consumed during a fire event.

The corresponding temperature of the internal compartmental gas layer due to the natural convection flow rates within the energy segment may reach approximately 910K (637 ^{o}C) after 3000 seconds (50 minutes). Due to internal gas temperatures and sustained degradation of the OEM battery Modules, the average internal wall temperature will approximately be 893K (620^{o}C). Due to the natural physics of the internal upper heated gas layer of a compartmental fire, it is assumed the upper 30% of the container is the primary radiated heat source. The theoretical centerline temperature of the associated smoke plume could reach approximately 917K (644^{o}C) at a height of 11 meters.

In this theoretical scenario, the worst case theoretical total radiant and convection heat flux on the target adjacent BESS located 10 feet across the passageway, assuming the peak wind velocity (1.92 m/s, 4.3 mph) based on local wind rose data will be approximately 12.2 kW/m^2.

While very unlikely based on the global ESS market sector of cascading fires between adjacent containerized battery energy storage systems, if a design basis fire event is realized and is unnoticed and unmitigated, an adjacent *ESS* Thermal Management System should be able to control the internal environment but could eventually shutdown when internal temperatures exceed pre-established setpoints (typically 90^{o}F/32 ^{o}C). Once the internal thermal management is no longer in operation, the heat transfer from the adjacent fully developed container fire could, as a function of the fire lifecycle and thermal insulation degradation, could exceed the thermal stability thresholds of the adjacent racks [6]. In the bounding scenario, and based on the best available information, the internal temperatures of the immediately adjacent BESS could experience a 160 ^{o}C increase.

The Acceptance Criteria governing this NFPA 551 Fire Risk Assessment is derived from the CFC where the design of the Starlight Project mitigates the probability of propagation from ESS Container to Container. Based on the information presented to Hiller, the convection and radiation heat transfer remains reasonably low. Refer to 20250320-SLS-AW0764-BOP-HMA-R0A for mitigation considerations [10].

Scope

This Fire Risk Assessment (FRA) identifies and quantifies the potential fire hazards associated with Starlight Solar Energy Storage Project (ESS) utilizing the *ESS* product line that is based on the OEM LFP module technology.

This Fire Risk Assessment was conducted in accordance with the requirements and guidelines of the:

- NFPA 551, *Guide for the Evaluation of Fire Risk Assessments* [11]
- SFPE G.04:2006 – *Engineering Guide: Fire Risk Assessment*; [12]
- SFPE-01 - SFPE Handbook of Fire Protection Engineering [13]
- ISO 16732-1: 2012 – Fire Safety Engineering – Fire Risk Assessment, Part 1: General[14]
- ISO 16732-3: 2012 – Fire Safety Engineering – Fire Risk Assessment, Part 3: Example of an Industrial Property [15]

Purpose and Objectives

The use of Lithium-ion (Li-ion) battery-based energy storage systems (ESS) has grown significantly over the past few years. In the United States alone, Li-ion battery (LIB) use has gone from 1 MW to almost 35,000 MW by the end of 2025 (refer to Figure 2) [16]. Many of these systems are smaller installations located in commercial occupancies, such as office buildings or manufacturing facilities. Yet, there has been relatively little research conducted on large commercial or industrial systems that can be used to ensure that effective fire protection strategies are in place.

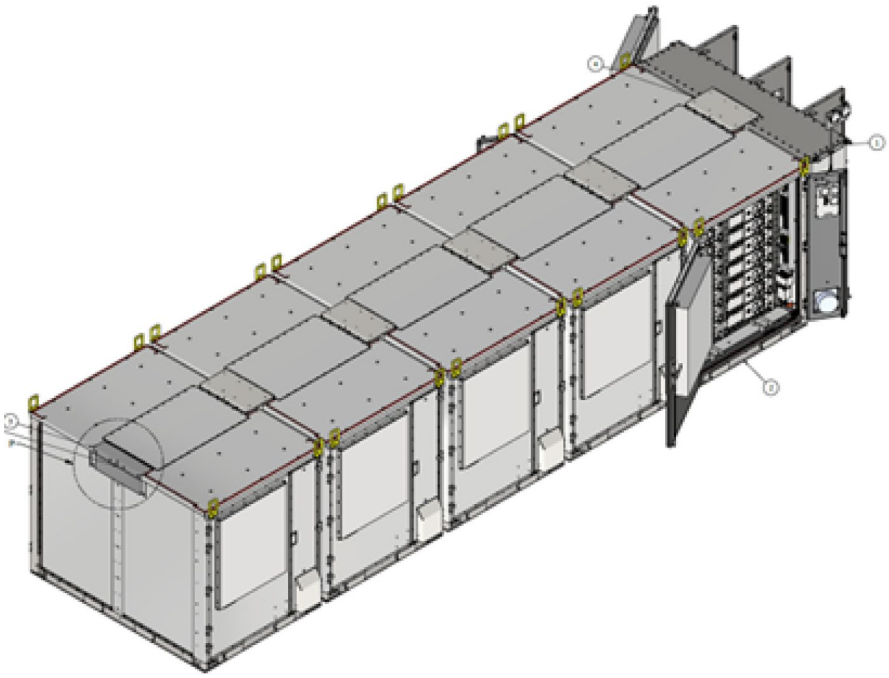

Figure 1: (assumed typ.) OEM ESS Design

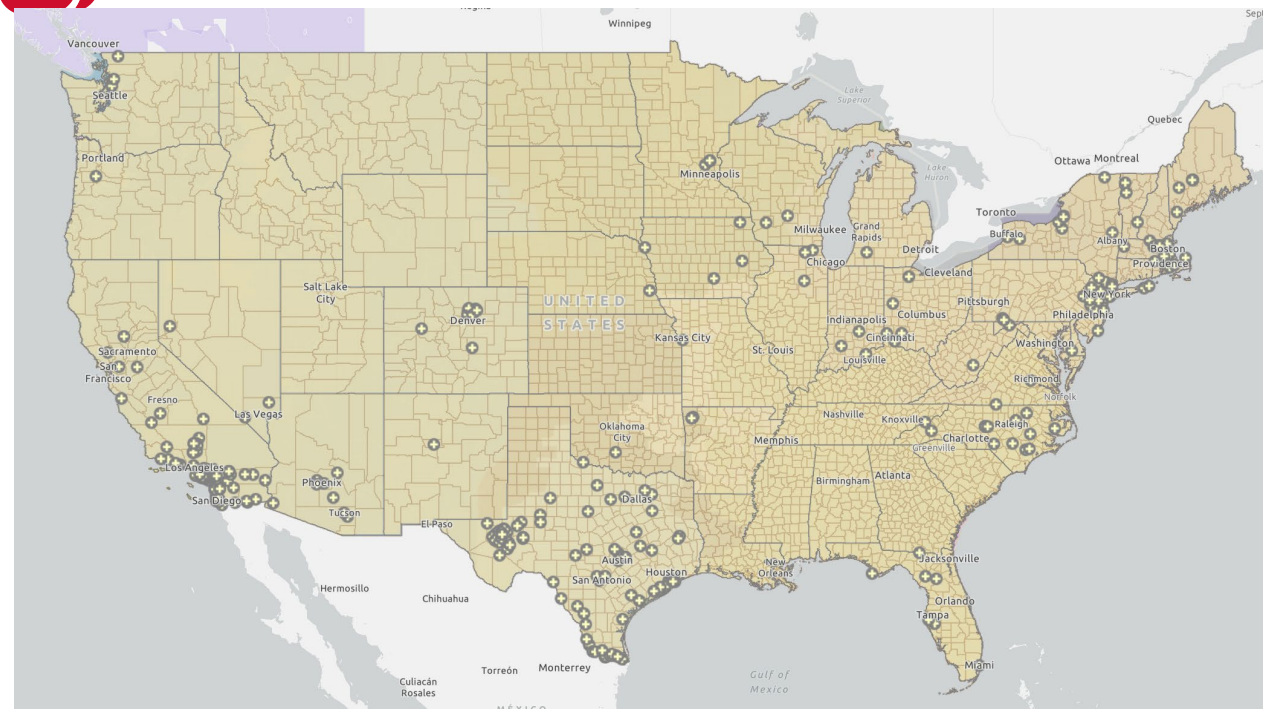

Figure 2: US Large Scale Battery Storage Installations by Region (2025) [17]

Many studies have addressed how failure of a single lithium-ion cell is affected by characteristics such as chemistry, electrolyte composition, state-of-charge (SOC), or format [18-26]. The subsequent propagation of thermal runaway to adjacent cells in a multiple cell battery module have also studied and characterized [7-9].

From a fire protection and fire risk perspective, the overall fire hazard of any ESS is a combination of all the combustible system components, including battery chemistry, battery form factors (e.g., cylindrical, prismatic, polymer pouch), battery capacity and energy density, state of change (SoC), materials of construction, and component design (e.g., battery, module). To ensure confidence in the resulting fire protection guidance, the ESS was assumed to be operating under a normal electrical operation where electrical abuse may typically occur, such that any proprietary electronic protection systems, e.g., battery management system (BMS), were limited in mitigative response. Any benefit from these proprietary systems would further reduce the overall hazard, (e.g., the likelihood of ignition), but is not necessary or sufficient to ensure the adequacy of the fire protection or response measures [27, 28].

It is recognized the OEM UL9540A Cell Level Report objectively indicated the establishment of thermal runaway producing 166.4 liters of flammable gas, of which approximately 75% is hydrogen. No external flaming was observed.

As part of this Fire Risk Assessment, the body of knowledge was researched, collected, reviewed, and summarized related to LIB ESSs to establish the technical basis for performance and any potential mitigation measures. The sources used include the Department of Energy (DOE) Safety Roadmap, relevant international consensus codes and standards, incident reports, related test plans, peer-reviewed research, and previous fire testing/research with the objective of identifying the inherent risks associated with the deployment of the LIB ESS technology to life (occupants or fire fighters) and for property (asset) protection.

Continuity of Operations is specifically excluded from this assessment as no administrative controls are assumed to limit the resultant hazard.

The literature review conducted as part of this Assessment is intended to identify potential knowledge or technology gaps in the information currently available.

Assessment Methodology

This Fire Risk Assessment and the format of this report employs both qualitative and quantitative methods to determine the inherent risks of the lithium-ion battery (LIB) energy storage system (ESS) technology and follows the guidance outlined in the SFPE Engineering Guide to *Application of Risk Assessment in Fire Protection Design* and the National Fire Protection Association (NFPA) Standard 551 *Guide for the Evaluation of Fire Risk Assessments* [11, 12].

The *SFPE Guide to Fire Risk Assessments* recommends the use of risk assessment methodologies in the design and assessment of building and/or process fire safety. This guide is a recognized and generally accepted and good engineering approach to fire risk assessments. The SFPE guide provides directions to practitioners in the selection and use of fire risk assessment methodologies used to determine adequacy of design for fire safety. It also provides guidance to project stakeholders in addressing fire risk acceptability. Furthermore, the SFPE guide establishes recommended processes to be considered for the use of risk assessment methodologies and provides references to available detailed sources of information on risk assessment methodologies, procedures, and data sources. However, the SFPE Guide to Fire Risk Assessments does not provide specific fire risk assessment methodologies or tools; nor does this guide provide specific data or acceptance criteria for use in the risk assessment process. Therefore, in the absence of specific quantification methodologies, the *SFPE Handbook of Fire Protection Engineering* [13] and the *Fire Protection Handbook* [29] as well as other peer-reviewed publications were used to identify the characteristic equations for calculating compartmental fires, heat release rates (HRRs), flammable gas temperatures, and surface temperatures.

The following figure outlines the process outlined in the SFPE Guide. The format of this report closely follows the recommendations of the SFPE Fire Risk Assessment Guide.

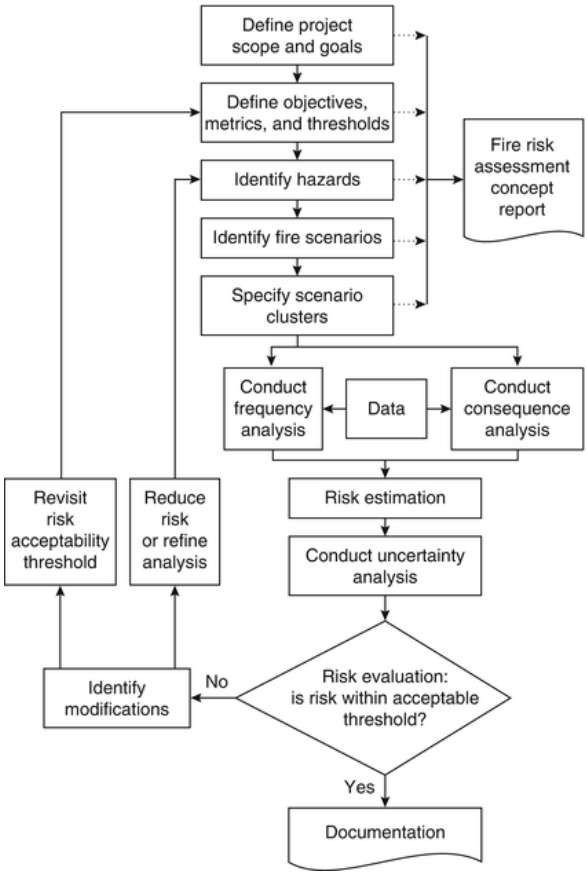

Figure 3: SFPE Fire Risk Assessment Process Flow Chart

Definition of the Project Scope

This BESS Level FRA was developed in support of the Empire II Starlight battery energy storage Project utilizing the *ESS*. The Starlight Project is located in proximity of 32.66016162785173, -116.28052568720432 as shown in Figure 4. The Starlight project will consist of eight (8) sections of DC Coupled Systems and will include clusters of ESS Energy Battery Storage Systems (BESS) interconnected with the electrical distribution system switchgear as shown in Figure 4 and Figure 5.

This project focuses on the inherent fire hazards and risks associated with the *ESS* lithium-ion battery (LIB) technology and limits the fire generated from the flammable gas emitted from one-Rack Level and determines the potential impacts to the surrounding adjacent structures [30]. This steady-state FRA leverages the qualitative information gained through an exhaustive literature review of the failure rates (the total number of failures within an item population, divided by the total time expended by that population, during a particular measurement interval under stated conditions) and consequences of LIB within the global ESS market sector, as well as calculates the heat flux generated from a fully engaged rack fire within a given ESS. In the absence of specific failure data of a manufacturer's part number, comparable and approximate reliability data presented in the Electronic Parts Reliability Database (EPRD), Non-electrical Parts Reliability Database (NPRD) or Failure Modes/Mechanisms Database (FMD).

This assessment does not quantify the increased pressures associated with system deflagrations of the vented flammable gases during LIB thermal runaway associated with the requirements of NFPA 68.

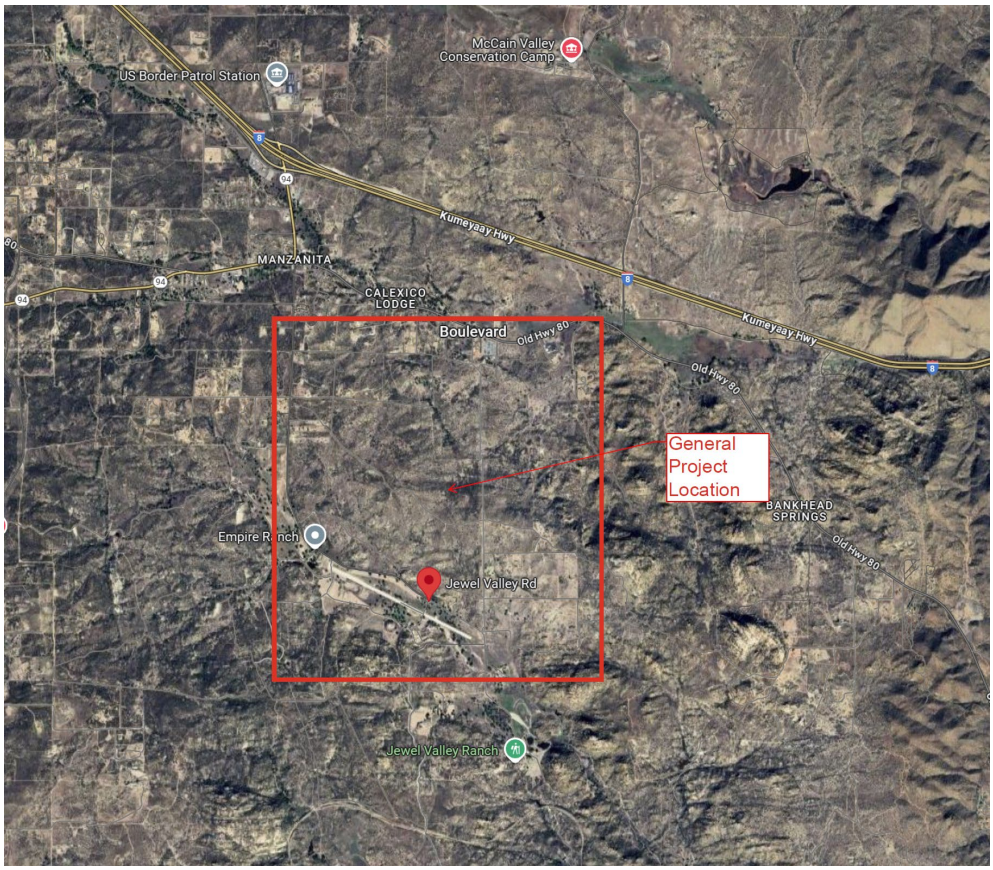

Figure 4: Starlight Project Site

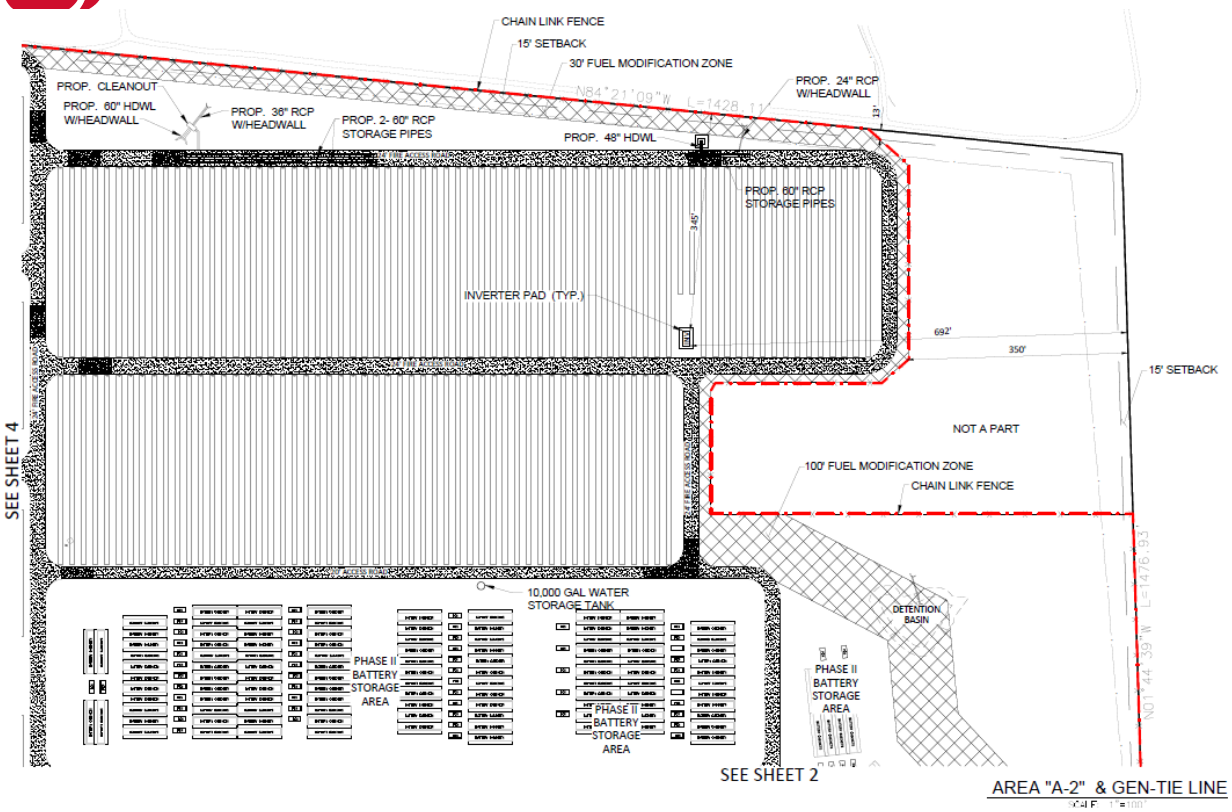

Figure 5: (Typ.) Starlight Project Layout

Analysis Enabling Assumptions

The following enabling assumptions were used to facilitate this Fire Risk Assessment to characterize a worst-case scenario:

- This NFPA 551 Fire Risk Assessment and Heat Flux Analysis is based on a theoretical energy storage system.
- Full compliance with NFPA 70 is field verified and documented accordingly.
- Although highly unlikely, a probabilistic initiating event of electrical abuse resulting in battery cell failure and subsequent cascading thermal runaway had to be assumed. This assumption is based on the UL 9540A Module Level Test Reports for the OEM cell and is used to bound the maximum theoretical fire event [7-9].
- First Responders reaction time is assumed to be less than 60 minutes based on the assumption of notification 30 minutes into the thermal runaway event and distance from San Diego Fire Authority Boulevarde Fire Station #47, 39223 CA-94, Boulevard, CA 91905 to Starlight Project Site (~1.1 miles). Alternatively, the distance from CAL FIRE White Star Fire Station, 1684 Tierra Del Sol Rd, Boulevard, CA 91905 to the Starlight site (4 miles).
- The UL 9540A test results for the OEM Module assemblies are assumed and result in failure of a single rack as recommended within NFPA 855 [31].
- Designed engineering controls for BMS or supplemental controls are assumed to be operable, but in a degraded condition and will not mitigate exothermic reaction.
- Non-Safety Integrity Level (SIL) controls and compensatory measures are not credited for accident mitigation.

- Rockwool (insulation material) thermal conductivity changes with increasing temperature. Therefore, the worst-case thermal properties are assumed (0.120 w/mK) [32].
- Ambient conditions are assumed to be standard pressure temperature (STP). External environmental air conditions assume a design basis wind of event of 1.92 m/s (4.3 mph). Ambient temperature is 295 K (22 °C/72 °F).
- Numerical/analytical methodologies employed are based on SFPE, NFPA Handbooks, or other peer-reviewed publications and are assumed to be adequate for characterizing the critical calculation variables and are cited herein.

Construction of the OEM Battery Cell

This BESS Level Fire Risk Assessment uses the best available information to characterize the risks associated with LIB technologies. It is recognized the *ESS* design has an integrated solution containing the OEM cell with a typical 3.2VDC, 280Ah technology as shown in Table 1 [7-9].

Table 1(typ.) LFP cell Data [7-9]

LFP cell	
Manufacturer	Typical
Model Number	
Chemistry	Lithium Iron Phosphate (LiFePo4)
Electrical Ratings	280 Ah, 3.2 V
Dimensions	207.5 x 173.7 x 72 mm
Weight	5420g
Construction Description	Prismatic, cell with UL approval
Tested to UL 1642	Yes
Tested to UL 1973	Yes

$LiFePO_4$ Battery Failure Mechanisms and Risks

As it pertains to the design and construction of the OEM battery modules, research of the failure modes and mechanisms of LiFePO4 cells was conducted as part of this analysis. It is assumed the published research on typical LiFePO4 failure mechanisms is comparable to the OEM cells. Therefore, the following discussion is based on comparable LiFePO4 battery chemistry and form factors to establish a technical basis upon which failure mechanics and performance characteristics could be extrapolated to support this analysis [7-9].

Research of the thermal performance of LiFePO4 cells demonstrates they have relatively comparable safety performance as other chemistries (LiCoO2, LiMn2O4, LiNiCoAlO2, LiNiO2, LiNiCoO2, LiNiCoTiMgO2) within the industrial energy storage market sector. However, Lithium-ion batteries have many advantages but the reactive, volatile and flammable materials present in the battery are a concern and may be a threat to auto-induced thermal runaway temperature and voltage [33]. As demonstrated by the OEM battery Modules during the UL9540A Module Level Test, overheating may start exothermal reactions that release even more heat which in turn can lead to an accelerated thermal runaway and propagation between cells. Research and industry experience indicates thermal runaway could be initiated due to overcharge, over-

discharge, mechanical deformation, external heating or an external or internal short circuit. The heat generated by any of these events may start exothermal reactions in the battery that in turn could lead to cell venting, fire or explosion [19, 33-36]. These risks are well known and are not only associated with the heat and high temperatures that may develop, the emission of harmful or poisonous gases also pose a danger that has been emphasized in literature but also other gases which can be flammable may be emitted. The reactions during overheating are typically due to the decomposition of the solid electrolyte interphase (SEI) layer, anode and cathode as well as electrolyte decomposition and combustion.

In general, when Li-ion battery failure is induced by thermal or electrical abuse, the failure eventually evolves into a thermal runaway [19]. The failures may be induced by external forces (i.e., severe mechanical shock or damage or internal/external thermal transients leading to damage), internal shorting (i.e., manufacturing induced defects, dendrite formation, metal particles, poison), or the poor thermal stability of Li-ion cells during uncontrolled overcharging or discharging [35]. Research has shown that when a number of LiFePO4 cells are used in a battery pack, there is always a disproportional *capacity distribution band* due to the individual battery state of charge, thermal performance, and "variation of capacity" between different cells [35]. This capacity band will continue to broaden throughout the battery pack as a function of the number of charging cycles, and eventually, the capacity of a battery pack will be limited by the cell with the lowest capacity. Thus, the lowest capacity cell will experience overcharge and over-discharge through the charging/discharging cycles. This has been proven to be the case, even if the whole pack is experiencing normal charge/discharge cycles, inducing electrical abuse and potentially leading to thermal runaway. Without a battery management system, the capacity band of a cylindrical Lithium-Iron-Phosphate (LFP) battery cannot be eliminated [19].

Although not specific to the OEM LiFePO4 cells due to the limitation of published information, research demonstrates that LiFePO4 cells within a battery pack or module are shown to degrade during testing [19, 34, 36, 37]. The research objectively indicates that LFP cell anode and cathode potentials create an environment where battery chemistry irregularities are formed within the anode, indicating the formation of an "iron bridge" between the anode and the cathode. The formation of these irregularities and the formation of dendrites create micro-shorting pathways during overcharge cycling conditions due to degraded cell capacity in the distribution band. Combining all results, the proposed possible failure mechanism occurs when oxidized iron (Fe) cations within the cathode develop during overcharge conditions and is then reduced during discharge. Simultaneous formation of dendrites within the anode during charging eventually creates an "iron bridge" that causes micro-shorting. Research indicates an increased rate of dendrite formation occurs in overcharge conditions than in the normal charging conditions [29-32].

Research of LiFePO4 cells indicates that as temperature increases above 60 ^{o}C, the Li-ion deintercalates from anode and the solid electrolyte interface film (SEI) layer of the lithium intercalated carbon anode undergoes an exothermic decomposition reaction. As the temperature continues to increase to about 105 ^{o}C, the SEI layer further decomposes where the cathode material generally loses its protection thereby exposing the electrolyte. Sustained exposures to temperatures above 100^{o}C facilitate system breakdown resulting in the initiation of exothermic reactions between the cathode active material and electrolyte resulting in rapidly increasing temperatures [38-40].

As the temperature increases, the separator of the lithium-ion battery degrades and thins. As the exothermic reaction continues, at temperatures above 180^{o}C the separator (polypropylene) degrades, thus reducing the protective properties between the positive and negative electrodes of the cell. This

results in the flow short circuit currents and the cell enters into the thermal runaway. As the internal temperatures increase to the range of 180–250°C, an exothermic reaction heat occurs between the lithium iron phosphate positive electrode and the electrolyte. At sustained temperatures above 200°C, the electrolyte decomposes, resulting in the release of significant heat from the exothermic reaction [35]. Generally, thermal runaway occurs when an uncontrolled exothermic reaction occurs. The exothermic reaction exponentially increases due to a surge in environmental temperature causing a further increase in internal cell temperature, which could without mitigation result in an explosion/deflagration. It is proposed that when temperatures are sustained above 150 °C, thermal runaway can occur spontaneously as a result of fire or explosion.

It is noted that the state of charge (SOC) is a significant contributing variable to the onset of thermal runaway of LiFePO4 cells. Other noted research indicates conditions where partially or fully discharged LiFePO4 cells, under adiabatic-like constant power heating similar to the UL9540A Module Level Test did not experience induced thermal runaway below 150°C [7-9]. Therefore, it is reasonable to assume that when the OEM LiFePO4 cells are partially discharged and incipient battery failure occurs, thermal runaway is unlikely.

Lithium-Ion Battery Hazards: Thermal Runaway – Causes and Results

Fire challenges associated with the bulk storage of Li-ion batteries are unique given the presence of a flammable organic electrolyte within the Li-ion battery as compared to the aqueous electrolytes typically found in other widely used battery types. As presented, when exposed to an external heat source (fire), Li-ion batteries can experience thermal runaway reactions resulting in the release of flammable organics and the potential rupture of the battery [41, 42].

The different stages and reactions contributing to the general thermal runaway process of a lithium-ion cell have been examined and are well documented within the energy storage industry [19, 33-36]. When a lithium-ion cell experiences thermal runaway, the noted degradation occurs resulting in elevated cell surface temperatures causing cascading impacts that have been demonstrated to propagate to the surrounding environment and adjacent cells. Observations from previous tests have shown these effects are very similar for all cell types (cylindrical hard case, pouch hard case, prismatic cell). Depending on the battery system design, adjacent cells may likewise be thermally damaged enter thermal runaway.

It is well documented that cell component breakdown due to thermal runaway results in the production of hot flammable gases due to the chemical reactions mentioned above. The flammable gas generation occurs during cell decomposition resulting in increased internal pressure, leading to cell expansion, including the application of compressive force to adjacent parts in the system. Depending on the magnitude of the expansive forces the cells have been known to rupture encapsulation.

Upon rupture, the cell begins to vent and together with the produced gas and a chaotic mixture of hot and glowing particles are ejected from the cell. Expelled particles typically contain pieces of active material from the cell's anode and cathode. Temperature measurement of released gases for the OEM LiFePO4 cells nominally 150 °C[7-9]. Analysis of the vented gas showed high proportions of hydrogen, hydrocarbon, and carbon monoxide. Therefore, flammability and the risk of deflagration or explosion, based upon industry performance is given at a fuel concentration of approximately 7.15% at ambient temperatures [7-9].

The mentioned effects usually have their impact on the battery and its environment as a function of time.

The heat release rate of a single LFP cell thermally interacts with adjacent cells increasing the internal temperatures and challenges the integrity of the cell within a module. This combination of effects creates an environment where subsequent cell failure will occur resulting in cascading degradation of the battery Modules [7-9]. Unmitigated, the entire module assembly will be damaged due to cell thermal runaway. The cascading degradations process will exponentially accelerate and usually within several minutes, the battery housing may lose integrity due to the amount of thermal energy [43, 44]. During degradation, the prismatic cells swell and bulge during pressurization and then safety vents are designed to release the internal pressure of the cell when a specified pressure is reached. Upon cell rupture, the gas accumulating inside the cell will be released and will react with atmospheric air (with fresh oxygen and moisture). "The air exchange with the battery will react with the freshly plated lithium metal and electrolyte and may cause explosion and ignition"[21].

The research associated with this FRA indicates the cell State of Charge (SoC) significantly and adversely impacts the reactivity of the cell during an external fire scenario. In particular, a fully charged battery has an increased propensity to undergo a thermal runaway reaction, increased initial fire growth rate and interestingly, decreased total energy release. This suggests that, to reduce the hazard potential in bulk storage, LIB should be well managed to avoid under/over-charging or being maintained at a reduced SOC [45].

MATERIAL	PEL (OSHA)	TLV (ACGIH)	%/wt.
Graphite	CAS# 7782-42-5 EC#231-955-3	None established	19,1
Lithium iron Phosphate	CAS# 15365-14-7 EC# 476-700-9	None established	37
Lithium Hexafluorophosphate	CAS# 21324-40-3 EC#244-344-7	Acute Tox. 3, H301; Skin Corr. 1B, H314;	3,2
Aluminium	CAS# 7429-90-5 EC#231-072-3	None established	4,6
Copper	CAS# 7440-50-8 EC#231-159-6	None Established	7,5
Ethyl Methyl Carbonate	CAS# 623-53-0 EC# 433-480-9	Inflammable, H225	12,2
Ethylene Carbonate	CAS# 96-49-1 EC#202-510-0	Eye Irrit. 2, H319	6,1

Figure 6:Typical Lithium ion LFP Battery MSDS

Lithium-Ion battery thermal and electrical abuse have been documented to result in exothermic reactions and runaway thermal events. There are a number of ways in which lithium-ion cells can be abused electrically, leading to cell thermal runaway reactions and include:

- Overcharge
- External Short Circuits
- Over Discharge

Overcharge

As presented, overcharge of a lithium-ion cell can cause significant degradation of both anode and cathode. Depending on cell chemistry, overcharge can cause anode plating rather than intercalation of lithium. Plated lithium forms dendrites that can grow over time and then cause internal shorting. Plated lithium also interacts exothermically with electrolytes. On the cathode, overcharge can cause excess removal of lithium from cathode material structures, such that their crystalline structure becomes unstable, resulting in an exothermic reaction. Reactions at both the anode and cathode, as well as lithium dendrite shorting can push a cell out of its thermal stability limits and result in a thermal runaway reaction. The more severe the degree of overcharge, the more likely the cell is to experience thermal runaway [46].

There are a few ways in which overcharge can occur. The most obvious mode of overcharge is charging a cell to too high of a voltage (over voltage, overcharge). For example, charging a 3.2 V rated cell above 5 V will likely lead to energetic failure. Charging at excessive currents, but not excessive voltages, can also cause an overcharge failure; in this case, localized regions of high current density within a cell will become overcharged, while other regions within the cell will remain within appropriate voltage limits [46, 47].

Although controlled through the Battery Management System (BMS), severe overcharge failures are not uncommon[48]. Unless the BMS is designed to meet Safety Integrity Level (SIL) Ratings, there is the potential a design or manufacturing defect can cause bypassing of protection mechanisms and result in severe overcharge failures. As noted in the report for the ESS used globally, these types of failures also occur as a result of human error with systems that either lack hardwired protection (e.g., prototype systems that are being tested) or in charging schemes with manual voltage and current settings [48].

Although severe overcharge will lead to cell thermal runaway, repeated slight overcharge of a cell may not cause a failure for an extended timeframe, but can eventually result in thermal runaway [21, 49]. Industry response to this known problem prompted requirements in IEEE 1725 and IEEE 1625 for cell manufacturers to communicate specific high voltage limits appropriate for secondary protection settings specific to each cell design to pack and device designers who purchase their cells. IEEE 1625 adopted the concept of safe charging current and charging voltage envelopes relative to temperature [46, 50, 51].

External Short Circuit

High rate discharging (or charging) can cause resistive heating within cells at points of high impedance as indicated in the findings associated with the ESS fires within the market sector [48, 52]. Such internal heating could cause cells to exceed thermal stability limits. Points of high impedance could include welding points within a cell (internal tab attachment) or electrode surfaces. As cell size and capacity increases, the likelihood of internal impedance heating leading to thermal runaway also increases. Larger cells exhibit slower heat transfer to their exteriors, and they usually have higher capacities. Thus, they have the potential to convert more electrical energy to internal heat. UN and UL testing requirements provide a minimum requirement for cell external short circuit resistance: discharge through a resistance of less than 0.1 ohm in a 55°C (131°F) environment. International and domestic shipping regulations (as found in the US CFR, as well as IATA and ICAO publications) require that cells or batteries be protected from short-circuiting. Investigation of a number of thermal runaway failures that have occurred during transport has revealed that improper packaging, particularly a failure to prevent short circuits, is a common cause of these incidents.

Over-Discharge

Research demonstrates over-discharging a lithium-ion cell to 0 V will not cause a thermal runaway reaction [43]. However, such over-discharge can cause internal damage to electrodes and current collectors, can lead to lithium plating if the cell is recharged (particularly, if the cell is repeatedly over-discharged), and can ultimately lead to thermal runaway [21]. Most BMS will allow the recharge of over-discharged cells, despite the potential for the negative electrode to become damaged [49]. Therefore, over-discharge does periodically cause thermal runaway of lithium-ion cells.

Forcing a cell into "reversal" (charging to a negative voltage, "forced over-discharge") may also cause thermal runaway. UL 1973 and UN tests provide a minimum requirement for resistance to forced over-discharge for cells used in multi- cell packs [53]. These tests are designed to simulate the most likely mechanism of forced discharge, which occurs when a cell with lower capacity than its neighboring series elements is present in a multi-series battery pack that is externally short circuited. A lower capacity cell of this type can occur due to aging of the battery pack. In this scenario, current flow from the higher capacity series elements in the pack will drive the discharged series element into reversal. The UN and UL testing does not include repeated forced discharge. Thus, if a system does not include protection electronics that will detect and disable charging of a damaged cell, it is possible a cell could be repeatedly forced over-discharged and ultimately undergo a thermal runaway reaction.

Thermal Abuse

The most direct way to exceed the thermal stability limits of a lithium-ion cell is to subject it to excessive external heating. Industry testing relies upon the use of an external heat source that is applied to the exterior of target cells to induce localized reactions and to determine if the failure propagates to the entire module [50, 54]. This literature review of the failure mechanisms of LIB indicates energetic field failures of LIB devices have been attributed to long-term operation of cells at temperatures just above the self-heating point of 70 to 90°C (158 to 194°F). Such failures require not only elevated temperature, but an adiabatic (highly insulated) environment, and extended times to reach a self-sustaining thermal runaway condition. If a ESS was exposed to long-term operation without environmental thermal management, significant damage could occur. Acute exposure of a cell to high temperatures will readily induce thermal runaway in that cell. As demonstrated in the UL9540A Module Level Test of the OEM MODULE Series battery module, if an internal cell fault is sufficient to cause thermal runaway in a single cell of a multi- cell battery pack, heat transfer from the faulting cell can cause thermal runaway in neighboring cells of the battery pack[55]. Thus, the thermal runaway reaction will propagate through a battery rack if there is a performance issue with the Thermal Management System.

Propagation of LFP cell thermal runaway has significant implications for fire suppression and fire protection. LIB in exothermic reactions self-generate oxygen to sustain the fire. A fire suppressant or low oxygen environment may extinguish flames from a battery pack, but the thermal runaway reaction will propagate if heat is not sufficiently removed from the adjacent cells[28]. Responding to fires involving lithium-ion battery packs have often described a series of re-ignition events. Typically, responders report they used a fire extinguisher on a battery pack fire, thought they had extinguished the fire, and then observed the fire re-ignite as an additional cell vented [47].

Risk Acceptability and Failure Initiation

Since May 2019, there have been over 69 documented stationary energy storage system fires within the

global market sector with greater than 26 occurring while the systems are in operation. Research has shown there are four main causes that have been attributed to ESS failures that include:

- Insufficient Battery Protection Systems against electric shock [48, 56, 57];
- Inadequate management of operating environment.
- Faulty Installations.
- Insufficient ESS BMS and EMS System Integration [48, 57, 58].

Based on the number of recent recorded industry failures, energy storage system Battery Management Systems (when designed as non- SIL) do not have a proven track record of fire mitigation/prevention due to thermal or electrical abuse. Research has objectively demonstrated that once the critical sustainment point of an exothermic reaction is reached, a Battery Management System cannot stop or mitigate the cascading failures of adjacent cells within modules [25, 41, 43, 49, 50, 54, 59, 60].

The National Fire Protection Association (NFPA) has conducted a series of tests to determine preferable suppression systems for ESS [61, 62] and determined that water based automatic sprinkler systems was chosen as a viable option for evaluating fire protection strategies for Li-ion batteries for lowering the exothermic reaction temperature. NFPA 13 does not provide a specific recommendation for the protection of Li-ion cells or complete batteries, and it is not known if water is the most appropriate extinguishing medium for Li-ion batteries. There is limited real-scale data available to support a fire hazard assessment of Li-ion based ESS and there is no experimental data available to support sprinkler protection guidance[27, 28, 41]. The ESS design intended for the Starlight Project does not include a fire suppression system, nor is one required. Present industry performance data objectively demonstrates through analyses and empirical testing, explosion control measures mitigate the greater risk.

Therefore, to determine the worst-case scenario it is assumed the ESS is experiencing a potential exothermic reaction and is suppressed results in a loss.

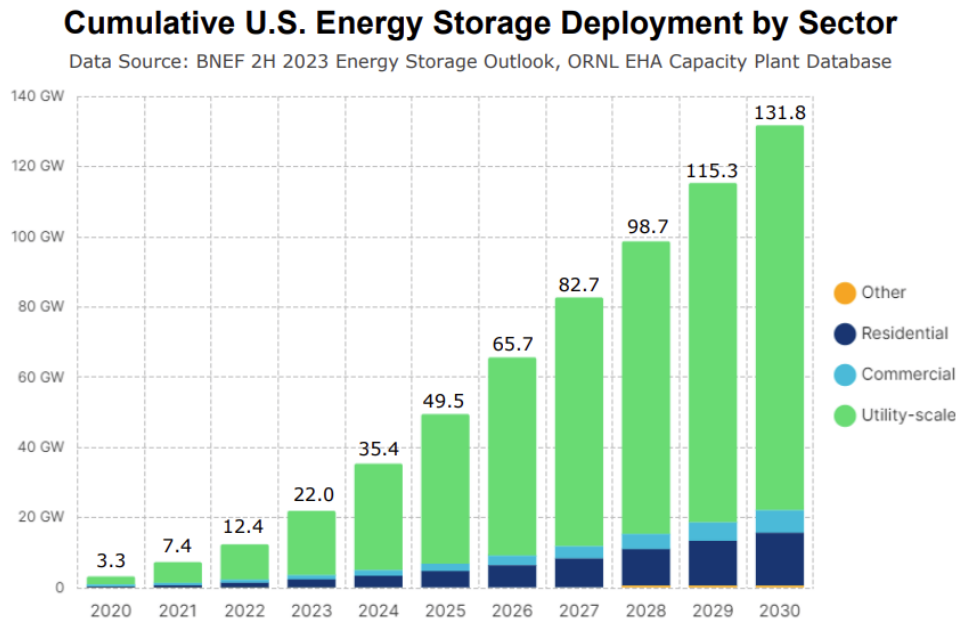

Figure 7: Global Energy Storage Project Projection [63]

Identification of the Hazards

The major hazards for large-scale ESS systems can be categorized as electrical, mechanical and other hazards. Electrical hazards occur when there is live contact between a person and an ESS system exposing the person to severe electric shocks. Mechanical hazards occur when there is an (unforeseen) physical collision between a person and an ESS system. Potential other hazards (mainly related to electric and electrochemical systems) include:

- Explosion hazards, caused by a rapid expansion of gases due to exothermic reaction and subsequent failure of LIB cells, Modules, Racks, and containers.
- Fire hazards arising from combustible materials used in the storage system.
- Thermal hazards, due to the thermal properties of a system or its components.
- Thermal runaway hazard, causing propagation of increasing temperatures, pressures, and fire towards neighboring cells.
- Chemical hazards, caused by (unforeseen) contact between a person and toxic, acidic, corrosive.
- Components leaking from the ESS system [64].

The risk of electrical shock at the system level should be mitigated by applying design rules regarding electrical insulation (e.g., containment), by wearing adequate personnel protective equipment and by imposing operational instructions. The risk of mechanical shock at the system level should be mitigated by applying design rules regarding enclosure design/construction. The risk of other hazards at the system level should be mitigated by applying design rules regarding containment.

To ensure safe handling in general, the following recommendations should be considered to prevent exposure to abusive environmental conditions:

- The ESS system or its components should not be opened or punctured, including during emergency operations.
- The ESS system or its components should not be left in places of high temperature.
- The ESS system or its components should not be exposed to condensation and high humidity and contact with water should be avoided.
- The ESS system or its components should not be submitted to excessive electrical stress [64].

Therefore, this Fire Risk Assessment bounds the aforementioned risks with the most conservative hazard that is a direct result of thermal defects within LIB resulting in the cascading impacts of exothermic reactions resulting in thermal runaway. Assuming conservative quasi-linearity of the published failure rates resulting in fire, the ESS may experience up to approximately 3% to 5% failures depending on the level of electrical and thermal abuse [52, 65]. However, while there is no readily identifiable industry research on failure of large-scale LFP systems, recent UL9540A testing of the LFP cells and modules objectively demonstrates a lower propensity of thermal runaway propagation.

Exothermic and Thermal Runaway Hazard Evaluation

Quantification of Heat Flux of an ESS Fire

Characterizing the fire hazards associated with the OEM containerized battery energy storage systems require an understanding of the amount of energy released during the exothermic reaction of a lithium-ion

battery (LIB) failure.

The potential cascading impacts associated with a fire in a lithium-ion battery ESS is significant based on the quantities of energy contained. Although the manufacturers like OEM utilized in the Battery Energy Storage System are certified and tested in accordance with UL9540 and UL 1973, the aforementioned fire safety features of the design is to prevent a catastrophic explosive event in a lithium-ion ESS. This FRA assumes the flammable gases have been ignited and results in a sustained steady-state fire.

The quantification of the radiant heat flux within ESS presents several challenges due to the unavailability of proprietary information. When available, specific manufacturer LIB data was applied. In absence of specific data, the "best available" information was used with an integrated standards-based approach with recognized and generally accepted good engineering practice. The conservative approach to radiant heat flux quantification is used to present a bounding. Understandably, proximity and adjacencies of siting and spacing of ESS containers contributes a significant role in fire safety.

The overall approach to the radiation heat transfer analysis of an ESS container fire is based on the cited works of the *SPFE Handbook of Fire Protection Engineering* for compartmental fires [13] and those of Quintiere's works in *Fundamentals of Fire Phenomena* [66] to calculate the following:

1. Effective Heat Release Rate (HRR).
2. Mass Flow Rate within the emitting (engaged) ESS.
3. Quantification of Peak Heat Release Rate of ESS Fire Event.
4. Temperature of the Internal Hot Gas Layer.
5. Internal and External Wall Temperature of the ESS Fire Source.
6. Smoke Plume Centerline Temperature.
7. Configuration View Factors.
8. Radiant Heat Flux.
9. Forced Convection Heat Transfer.
10. Wall Temperature of Target ESS and the site perimeter.
11. Internal Temperature Increase of Adjacent Target ESS.

Effective Heat Release Rate (HRR) of LIB in a ESS

The energy release rate (heat release rate, HRR) of the compartmental fire is based on UL 9540A testing and assumes sustained peak based on the UL9540A cell level test data and is extrapolated to numerically characterize a worst-case scenario [7-9].

The heat release rate is the recognized single most important variable in a fire hazard [66]. It is the rate at which the combustion reactions produce heat. The relationship of these two quantities can be expressed as

$$HRR = \Delta h_c * MLR$$

Where Δh_c is the effective heat of combustion and MLR is the Mass Loss Rate of the LIB. The mass loss rate (burning rate) of the battery is an essential element in quantifying the heat release rate; however, in comparison to the volumetric flow rates within the compartment, the mass loss rate plays a somewhat insignificant role in the total heat release rate.

Therefore, the mass flow rate of air and the heat of combustion of lithium-ion batteries combusting in air is used to approximate the peak heat release rate. A typical prismatic LIB has an average mass of nominally 5.4 kg and a MLR of 0.0015 kg/s and is assumed for all LFP cells as there is no published data on the OEM MODULE prismatic [49, 67, 68]. Based on cell and unit Level UL9540A tests, it is assumed that conservatively, 10% of the mass of the module was consumed during the test [7-9].

The effective heat of combustion (Δhc) for a LIB is the heat of combustion which would be expected in a fire where incomplete combustion takes place. The effective heat of combustion is often also described as a fraction of the theoretical heat of combustion [13]. The effective heat of combustion assumed for this analysis is based on the *Thermal runaway and safety of large lithium-ion battery systems* and the Underwriters Laboratory UL 9540A testing of the OEM cells [7-9]. The range of values used for this analysis is based on the interpolated data presented in the UL 9540A cell Level Test and is assumed to be 24.2 kJ/kg for the fully engaged Rack as well as the upper range of identified effective heat of combustion [68, 69].

Mass Flow Rate within the emitting (on fire) ESS

Compartment fires with forced ventilation can significantly impact the fire growth, temperature within the compartment, spread of gases from the fire, and the decent of the smoke layer within the compartment [13]. This Fire Risk Assessment assumes naturally occurring convection due to internally heated fire dynamics to establish a bounding scenario.

This scenario analyzes compartmental fire growth of the fire will be significantly impacted by the volumetric air flow rate within the ESS container by providing an adequate oxygen supply for the large quantity of fuel. However, it also serves as a limiting factor for the peak heat release rate of a fire in a compartment with uniform air flow.

Naturally ventilated fires typically have a stratified thermal hot gas layer that develops from the fire plume and descends toward the floor as the oxygen concentration is reduced within the compartment. However, a forced ventilation compartment may have an unstable gas layer due to the mixing of the combustion products and the air flow which spreads the hot gases throughout the compartment [13].

As in any compartment fire, the depth of the smoke layer increases over time. However, the smoke layer in forced ventilation scenarios descends until it reaches equilibrium; this phenomenon allows for additional fuel to be consumed. Once the fire reaches its peak heat release rate, the fire growth is limited to the ventilation rate throughout the compartment. Since the ventilation rate is constant, the amount of fuel that can be consumed per second becomes constant, allowing the fire to reach a steady-state condition until all fuel within the container is consumed [13].

The mass flow of the burning fuel is given as the ratio of the fire energy release rate and the effective heat of combustion and is quantified by

$$m' = \frac{Q'}{\Delta h_c} + m'_{air}$$

Where,
Q' is the fire energy release rate.
Δh_c is the effective heat of combustion.
m'_{air} is the mass flow of the forced ventilation.

Derivation and Extrapolation of Fuel for Design Basis Fire Event

To establish the bounding scenario of the Design Basis Fire Event the flammable gas, mass loss, smoke and release rates presented in the UL 9540A Cell, Module and Unit Level Tests was used [7-9]. However, it is noted that critical information that is typically presented in the UL9540A Module Level tests including the flammable gas constituents and mass lost during the test was not available for this analysis. Therefore, as a matter of sound engineering practice, Hiller engineers linearly extrapolated the UL9540A Cell Level data to establish the theoretical fuel consumed for the design basis fire event.

The UL9540A:2020 Unit Level Test indicates the 3 damaged cells and the induced TRA duration with a nominal duration of 66 minutes.

Understanding the great variability of fires where no two fire events are identical, as part of establishing the bounding conservative design basis fire life cycle, the scenario assumes the fire occurs more rapidly, burns longer, and consumes more fuel. Specifically, it is assumed the mass loss of a Module during a thermal runaway event was conservatively set at 10% [7-9]. Given the documented energy density of typical LFP cells and the total extrapolated mass lost during a TRA event for Unit, it is conservatively assumed that 10% of the total fuel load is consumed for a peak 3000 seconds to establish the maximum theoretical heat release rate (HRR) and heat flux to the environment.

Quantification of Peak Heat Release Rate of ESS Fire Event

The HRR is defined as “the rate at which energy is generated by the burning of a fuel and oxygen mixture”. As the heat release rate increases, the heat, smoke production and pressure within the area will increase and spread along available flow paths toward low pressure areas. The most common method of quantifying the heat release rate is through Oxygen Consumption Calorimetry (OC), which assumes that the HRR is proportional to the oxygen consumed during the combustion of common organic fuels. However, quantifying the heat release rate through OC methods is challenging for lithium-ion batteries due to their ability to release oxygen during failure. LIB’s produce sufficient oxygen during the exothermic reaction to sustain a flame [47, 61, 62].

The heat release rate of a LIB ESS fire is interdependent on the initiating event, status of the LIB charging/discharging the quantity of fuel, environmental conditions, and the status of the ventilation conditions [46, 47, 61, 62]. To bound the conditions for determining the peak heat release rate, it is assumed to be limited to the forced-ventilation air flow within the compartment. Based on industry research on the failure mechanics of thermal runaway in large lithium-ion battery systems, the effective heat of combustion of a lithium-ion battery in air was determined to be approximately 24.2kJ/kg [41, 43, 44, 49, 50, 59]. It is well published that the mass flow rate of the gas layer within the compartment is dependent on the mass loss rate of the fuel (kg/s), density of air (1.2 kg/m3) and the range of volumetric airflow rates (m^3/s). For the purposes of this FRA, based on the system integrators information on HVAC performance, the ventilation rate is used to determine the peak heat release rate.

Although it is generally understood that it is uncommon for LIBs to reach full combustion; for the purpose of bounding a quantifiable fire risk, it is assumed the combustion efficiency for oxygen containing products can be between 90 and 100%.

Therefore, the mass flow rate of the flammable gas compartmentalized fires is dependent on the temperature, density of the air, and the volumetric flow rate of the mechanical ventilation system in addition to the mass loss rate of the fuel (rate of volatile release from LIB failure) which is mechanically combined to form the mixed flammable gas layer. It is also assumed fire engagement is the initiating source for volatile gases. The failure of any other system, structure, or component concurrent with a LIB fire event is assumed to be beyond extremely unlikely.

As part of the quantification of the peak energy released during a LIB exothermic reaction, the mass loss rate of the battery has been determined although important, in comparison to the volumetric flow rates within the compartment, the mass loss rate is nearly negligible. Both are quantified in this analysis for consistency. Therefore, the mass flow rate of air and the heat of combustion of lithium-ion batteries combusting in air is used to approximate the peak heat release rate where,

$$\dot{Q} = \Delta H_{eff} * \dot{m}$$

Where,

$$\dot{m} = \dot{m_{air}} + \dot{m}_{LIB} = \left(\rho_{air} * \dot{V}\right) + MLR_{fuel}$$

ρ_{air} is the density of air
$\dot{V}$ is the volumetric flow rate
MLR_{fuel} is the Mass Loss Rate of the LIB

Once the peak heat release is reached, the ESS compartment is assumed to be fully developed/engaged. A normalized time of 3000 seconds (50 minutes) is assumed, and cascading impacts of exponential temperature increases to consume the rack. The Design Basis Accident scenario assumes a steady state exothermic reaction is sustained until a large percentage of the lithium-ion fuel is consumed and is bound by the energy within a single rack as specified by NFPA 855.

The components of a LIB fire and the associated release of volatile gases of the sustained exothermic reaction is due to the thermal breakdown of the cells and module includes the separators, packaging, and electrolyte of LIBs. The gases potentially vented during a thermal runaway reaction may include:

- Acetylene
- Ethylene
- Methane
- Methanol
- Propane
- Formaldehyde
- Hydrogen Bromide
- Hydrogen Chloride
- Hydrogen Fluoride
- Carbon Dioxide
- Carbon Monoxide
- Ammonia
- Hydrogen Cyanide
- Hydrogen [69-71]

With the large quantity of batteries and corresponding energy stored within these systems, a large amount of fuel and flammable gases will be generated during exothermic reaction leading to a potential

deflagration. Recent analysis indicates, as a function of battery failure mechanics, each ESS could emit approximately 61,443 L of flammable gases may be released during a single rack event [25, 44, 47, 49, 50, 69, 72].

For the purpose of establishing bounding conditions for this Fire Risk Assessment, it is reasonable to assume that flammable volatiles will continue to be released from failing cells even after the peak heat release rate has been reached. As the temperature continues to rise in the containerized ESS, excess unburnt fuel vapors will continue to be released contributing to the temperature increase of the gaseous mass within the container. With these enabling assumptions the calculated peak Heat Release Rate for the *ESS* is approximately 16.4 MW.

Internal Temperature of the Hot Gas Layer

Research conducted for this FRA has identified recommendations from the *SFPE Fire Protection Engineering Handbook* [29] as a suitable method for calculating the temperature rise of the upper gas layer in a compartmentalized fire using the method of McCaffrey, Quintiere, and Harkleroad (MQH) [29]. The MQH method applies the conservation of energy principle to the hot gas layer, which is determined by the following

$$\frac{\Delta T_g}{T_\infty} = \frac{\frac{\dot{Q}}{\dot{m}_g c_p T_\infty}}{1 + \frac{A h_g}{\dot{m}_g c_p}}$$

Where
$\frac{\Delta T_g}{T_\infty}$ is the Change in Temperature above ambient overtime
$\dot{Q}$ is the Heat Release Rate (kW)
$\dot{m}_g$ is the Mass Flow Rate of gas layer (kg/s)
Cp is the Specific Heat of Air (kJ/kg-K)
T_∞ is the Ambient Air Temperature (K)
h_g is the Heat Transfer Coefficient (kW/m^{2}K)
A is the Surface Area of Compartment Boundaries

The MQH methodology facilitates the analyzation of the compartment temperature with respect to the energy generated by the fire, the flow rate of the gas out an opening under natural ventilation ($\dot{m}_g$), the specific heat of the air (c_p), and the heat lost from the hot gas layer to the surrounding surfaces (h_g) [13, 68]. For the purposes of this FRA, it is assumed that ventilation is achieved through inherent design losses within the engaged containerized ESS.

Lithium-ion batteries challenge this ventilation-limited premise as sufficient oxygen is generated through the exothermic reaction for sustainability [25, 46, 49, 61, 62, 73]. Testing has shown that lithium-ion cells are capable of producing sparks of flaming combustion in an inert environment along with the release of significant quantities of flammable gases. Therefore, it is assumed that a substantial amount of oxygen can be released during each cell failure as a result of the decomposition of the battery's metal oxide (cathode). It is also assumed a limited oxygen concentration within the container will not stop the progression of thermal runaway within the ESS. Recent studies of LIB failures have indicated that when the ambient temperature reaches the battery thermal stability limits (typically 160 °C) thermal runaway propagation may occur more readily. Although the oxygen released from the individual cells may not be sufficient to

sustain steady combustion within a ventilation-limited compartment, masses of flammable gases from the thermal runaway reactions of LIB's will continue to be released. If the container is breached, sufficient oxygen may enter the container resulting in a deflagration of flammable gases [13, 29].

The likely scenario poses over-pressurization and explosion hazards due to the mass of unburnt fuel in a closed unventilated compartment; this presents additional hazards that are outside the scope of this analysis.

Therefore, based on the assumption that forced ventilation will be used to mitigate hazards posed by lithium-ion cells during failure, a forced ventilation scenario can be used to characterize a fully developed fire within an ESS. The continuous air flow into the ESS container will allow the fire to be limited to the quantity of fuel within the compartment – representing a fully-involved ESS fire event.

The hot gas layer temperature is largely impacted by the ventilation conditions within the compartment. Therefore, with the understanding of the MQH methodology constraints, it is refined by the application of the work of Foote, Pagni, and Alvares. Foote, Pagni, and Alvares conducted a series of 64 fire tests with varying forced ventilation conditions [13]. From these tests, empirical constants that represent the change in the hot gas layer temperature in forced ventilation conditions were derived. Applying the MQH method, Foote, Pagni, and Alvares added data for forced ventilation fires – now referred to as the FPA method was applied to calculate the temperature of the gas layer through,

$$\frac{\Delta T_g}{T_\infty} = 0.63 \left(\frac{\dot{Q}}{\dot{m}_g c_p T_\infty} \right)^{0.72} \left(\frac{A h_g}{\dot{m}_g c_p} \right)^{-0.36}$$

The calculated ESS internal temperature of the heated upper gas layer could reach 910 K (637°C) after nominally 3000 seconds and is assumed to be suspended in the upper third of the battery compartment thereby heating the internal surfaces.

Internal Wall Temperature of the ESS Fire Source

The approach to calculating the wall temperature follows the *SFPE Fire Protection Engineering Handbook* [29] for compartmentalized fires and applies the work of Peatross and Beyler for highly conductive materials. Peatross and Beyler refined the MQH method based on the assumption normal insulating materials will have negligible impact on the total heat released during a fully engaged fire with highly conductive walls. Therefore, although the Peatross and Beyler ignores insulation of the container walls. This FRA follows the precedence and recognizes the existence of insulating materials but bounds the total risk through the application of Peatross and Beyler method.

The rise of the wall temperature of the container is a function of the heat transfer between the hot gas layer, insulation, and the steel panel. The temperature of the panel is a function of the heat stored within the panel with respect to the steel's material properties (density, specific heat, thickness, surface area). The rise in the wall temperature is dependent on the enthalpy flow through the wall – heat into the wall from the developed compartment fire and the outflow of heat from the wall to the external ambient environment. The gas layer throughout a mechanically ventilated compartment is assumed to be uniform, which heats the boundary layers (walls) at a constant rate.

$$m_w^{"} c \frac{dT_w}{dt} = h_g(T_g - T_w) - h_\infty T_w$$

The Peatross and Beyler heat flow into the wall from the radiant and convective heat from the hot gas layer and the heat outflow of the convective losses from the wall to the outside. According to Quintiere's *Fundamentals of Fire Phenomena* [66], the temperature rise of the ESS wall is calculated through the application of

$$\frac{dT_w}{dt} = \frac{1}{\rho_s c_s A_w \Delta x}\left[\varepsilon\sigma(T_g^4 + T_W^4) + h_{hot} A_W (T_g - T_w) - h_\infty A_w (T_w - T_\infty)\right]$$

Where,

$\frac{dT_w}{dt}$ is the change in wall temperature above ambient over time
ρ_s is the density of the container wall steel plate
$\boldsymbol{c_s}$ is the specific heat of steel
Δx is the thickness of the steel plate
A_w is the area of the containerized ESS exposed to the hot gas layer
ε is emissivity
σ is the Boltzman's Constant
T_g is the temperature of the gas layer
T_∞ is the ambient temperature
T_w is the temperature of the wall
h_{hot} is the heat transfer coefficient (hot)
h_∞ is the heat transfer coefficient (ambient)

Heat Transfer Coefficient

To quantify the convective heat transfer at the boundary layer between the hot gas layer and the compartment walls, an effective heat transfer coefficient must be calculated following the guidance of Peatross and Beyler. A heat transfer coefficient quantifies that rate at which heat is transferred from the hot gas layer of the fire through the solid wall [74]. This following equation represents a heat transfer coefficient that is a function of the temperature dependent thermal conductivity of the steel panel, density, and specific heat of the steel with respect to time [75].

$$h_{wall.ext} = \sqrt{\frac{kpc}{t}}$$

Where,
k = thermal conductivity (kW/m-K)
p = density of steel (kg/m3)
c = specific heat (kJ/kg-K)
t = time (s)

Under ambient conditions, the heat transfer coefficient is a stagnant value, which is used to represent the convective losses to the outside of the container. This heat transfer coefficient is a function of the thermal conductivity of the steel at ambient condition and the thickness of the steel. Understanding the thermal insulation limitations of the Rockwool panels, limited credit is applied for the insulation resistance value.

Fire/Smoke Plume Centerline Temperature

A characteristic accompanying the phenomenon of an ESS fire, especially in compartments in the phase of its development, is Fire Plume. For various reasons, the subject of concern may be the determination of an incipient smoke temperature. From the point of view of the methods used and extent of details, the temperature analysis of smoke and Fire Plume may be quite variable and challenging to determine. However, publications evaluated for this Fire Risk Assessment has identified the following methodology for calculating the centerline temperature for a smoke/fire plume as follows [20, 76]:

$$\Delta T_{osa} = 0.0964 \left(\frac{T_\infty}{g\ c_p^2\ \rho_o^2} \right)^{\frac{1}{3}} Q'^{\frac{2}{3}}_k (z - z_0)^{-\frac{5}{3}}$$

Where,
ΔT_{osa} is the smoke plume centerline temperature
T_∞ is the ambient temperature
g is the gravitational constant
c_p gas specific heat capacity
ρ_o ambient air density
Q'_k heat flux shared by convection
z height above the inflammable material surface
z_o Fire Plume virtual start

Understanding the plume centerline temperature is an important characteristic that contributes thermal radiation heat transfer to the adjacent containers and to the calculation of the ground level surface temperatures. The centerline temperature of the anticipated plume (propane equivalent) is approximately 917 K (644 °C) at an elevation of 11 meters.

Configuration/View Factors

A configuration factor is a purely geometrical relation between two surfaces, and is defined as the fraction of radiation leaving one surface which is intercepted by the other surface [13]. This factor is the variable that determines the fraction of radiation received by the target, with respect to the total radiation emitted from the source. The view factor accounts for the shape, orientation, and size of both the emitter and the target as well as the separation distance between them. Since this model accounts for the radiation coming from the heated ESS container and the externally vented flames, two view factors are calculated. Therefore, the incident radiant flux from a ESS fully engaged rack fire (source) to an adjacent ESS (target) separated by a given distance *x*, is given by

$$\ddot{q} = \tau E F_{12}$$

Where E is the emissivity of the transmitting medium, and F is the view factor between the source and the Target and τ is the atmospheric attenuation due to water vapor and carbon dioxide. In this case, the view factor will be the integration of the emitting side of the target and the energy emitted from escaping hot gas. It is assumed the hot gases will escape around the doors of the source and will form a pseudo-cylindrical shape. Secondly, the side of the source that radiates the thermal energy to the adjacent ESS is as indicated in Figure 8.

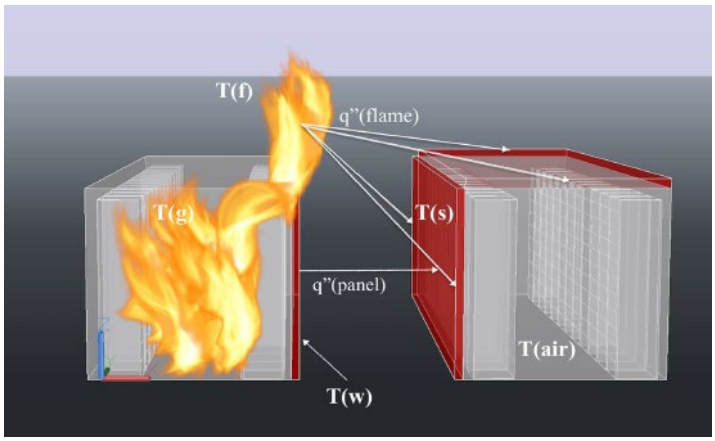

Figure 8: Application of Focus Factors [68]

The view factor from the ESS radiant source to adjacent containers is a critical component of this radiation heat transfer analysis. It is within this factor that the various separation distances are accounted for. Intuitively, the radiated heat is inversely proportional to distance: a fire's intensity reduces with distance. The view factors account for the angle, separation distance, area of radiating surface/flame and the area of the target surface. The view factors for the radiating panel and cylindrical vented flames are calculated through the methods shown as follows:

Determining the geometry for the identical, parallel, directly opposing ESS containers is taken from the *SFPE Fire Protection Engineering Handbook* [29] where

$$F_{plates} = \left(\frac{2}{\pi XY}\right)\left[ln\sqrt{\frac{X_1 Y_1}{1+X^2Y^2}} + X\sqrt{1+X^2} * tan^{-1}\left(\frac{Y}{\sqrt{1+X^2}}\right) - Xatan(X) - Yatan(Y)\right]$$

And

$$X_1 = 1 + X^2$$

$$Y_1 = 1 + Y^2$$

X is the ratio of width to length of the ESS
Y is the ratio of height to length of the ESS

The view factor from the escaping hot gases is determined by its vertical and horizontal components by

$$F_{cycl.flame.vert} = \frac{1}{\pi S} * \text{atan}\left(\frac{h}{\sqrt{S^2+1}}\right) - \frac{h}{\pi S} * atan\left(\sqrt{\frac{S-1}{S+1}}\right) + \frac{Ah}{\pi S\sqrt{A^2-1}} * atan\left(\sqrt{\frac{(A+1)(S-1)}{(A-1)(S+1)}}\right)$$

And

$$F_{cycl.flame.horiz} = \frac{\left(B - \frac{1}{s}\right)}{\pi\sqrt{B^2 - 1}} * \text{atan}\left(\sqrt{\frac{(B+1)(S-1)}{(A-1)(S+1)}}\right) - \frac{A - \frac{1}{S}}{\pi\sqrt{A^2 - 1}} * atan\left(\sqrt{\frac{(A+1)(S-1)}{(A-1)(S+1)}}\right)$$

Where the separation distance between the cylindrical radiant body (L), and the size of the flame (diameter (D) and flame height (Hf)) and,

$$S = \frac{2L}{D}$$

$$h = \frac{2H}{D}$$

$$A = \frac{h^2 + S^2 + 1}{2S}$$

$$B = \frac{1 + S^2}{2S}$$

Total Radiant Heat Flux

As noted, the radiant heat flux between containers is determined by the derivation of $\ddot{q} = \tau E F_{12}$, therefore determining the total incident radiative heat flux emitted from the ESS fire source is a summation of the heat flux from the flame and the heat radiated from the steel panel. The radiant heat flux emitted by the heated panel of the ESS fire source is quantified by the correlation shown in the equation below.

$$\dot{q}_{panel.rad} = \varepsilon\sigma F_{1p,2p}(T_w^4 - T_\infty^4)$$

And

$$\dot{q}_{cyl.rad} = \varepsilon\sigma F_{1c,2c}\left(T_{fl}^4 - T_\infty^4\right)$$

Where,

ε= emissivity of surface
σ = Stefen-Boltzmann Constant
$F_{1p,2p}$ = View factor from parallel ESS steel panels
$F_{1c,2c}$ = View factor from cylindrical flame exiting ESS to exposed ESS steel panel
T_w = Wall temperature of flames exiting the fire source ESS
T_{fl} = Flame temperature of flames exiting the fire source ESS
T_∞ is the ambient temperature

Wall Temperature of Target ESS and Radiant Heat Flux

Determining the magnitude of the incident radiation exposure on the target ESS, the quantity of radiation absorbed into the adjacent steel panels is calculated as follows:

$$T_{adj.ESS.surface} = \sqrt[4]{\left(T_{wall.ext}^4 - \frac{\dot{q}_{total.rad}}{\sigma}\right)}$$

Although the steel OEM enclosures are noncombustible, they have a high thermal conductivity – the property of a material to conduct heat. As the steel heats up, its thermal conductivity is reduced, lessening its strength, which allows the heat to be transferred through the panel more quickly. Therefore, as the fire grows within the ESS fire source, higher radiant heat fluxes will be emitted and absorbed into the target ESS over time, which will raise the temperature of the steel panel.

Therefore the net heat received at the adjacent target surface is determined by [77].

$$\dot{q}''_{rec.adj.ESS} = \varepsilon\left(\dot{q}_{ESS.total} - \sigma T_{adj.ESS.surface}^4\right)$$

Wind Driven Thermal Radiated Heat Transfer and Surface Level Analysis

A conservative 1.92 m/s (4.3mph) Wind Driven Event ground level (surface) temperature due to thermal radiation heat transfer is assumed and is based on the average wind presented in Figure 11. The Wind Driven Event is calculated assuming the ESS container could be compromised due to the internal heat and fire during an exothermic reaction.

If there was a breach in the container integrity resulting in a release of a smoke/fire plume, the centerline temperature of the fire/smoke plume would be calculated using the following numerical analysis outlined in *SPFE Handbook of Fire Protection Engineering* for compartmental fires [13] and those of Quintiere's works in *Fundamentals of Fire Phenomena*:

$$\Delta T_{osa} = 0.0964\left(\frac{T_\infty}{g\ c_p^2\ \rho_o^2}\right)^{\frac{1}{3}} Q'^{\frac{2}{3}}_k (z - z_0)^{-\frac{5}{3}}$$

Where,
ΔT_{osa} is the smoke plume centerline temperature
T_∞ is the ambient temperature
g is the gravitational constant
c_p gas specific heat capacity
ρ_o ambient air density
Q'_k heat flux shared by convection
z height above the inflammable material surface
z_o Fire Plume virtual start

The magnitude of the incident thermal radiation exposure on the surface, the quantity of radiation absorbed into the ground (assumed black body) would be calculated using the Mudan Method [13]as follows:

$$q'_{plume} = EF\tau$$

Where
E is the average emissive power of the plume at the flame surface
F is the view factor to the target
τ is the atmospheric transmissivity.

The thermal power of the flame is given by

$$E = E_{max}e^{-sD} + E_s[1 - e^{-sD}]$$

Where,
E_{max} is equivalent blackbody emissive power, 140 kW/m^2
s is the extinction coefficient, 0.12 m–1
D is the diameter of the fire
$E_s$is the emissive power of smoke, 20kW/m^2

The view factor of the wind driven fire/smoke plume is determined by

$$F = \sqrt{\pi {F_v}^2 + \pi {F_H}^2}$$

Where,

$$\pi F_v = \frac{a\cos\theta}{b - a\,sin\theta}\,\frac{a^2 + (b+1)^2 - 2b(1+sin\theta)}{\sqrt{AB}}\,tan^{-1}\left(\sqrt{\frac{A}{B}}\left(\frac{b-1}{b+1}\right)^{\frac{1}{2}}\right) + \frac{cos\theta}{\sqrt{C}}\,x\left[tan^{-1}\left(\frac{ab - (b^2-1)sin\theta}{\sqrt{b^2-1}\sqrt{C}}\right) + tan^{-1}\left(\frac{(b^2-1)sin\theta}{\sqrt{b^2-1}\sqrt{C}}\right)\right] - \frac{a\cos\theta}{(b - a\,sin\theta)}\,tan^{-1}\left(\sqrt{\frac{b-1}{b+1}}\right)$$

And

$$\pi F_H = tan^{-1}\left(\sqrt{\frac{b-1}{b+1}}\right) - \frac{a^2 + (b+1)^2 - 2(b+1+absin\theta)}{\sqrt{AB}}\,tan^{-1}\left(\sqrt{\frac{A}{B}}\left(\frac{b-1}{b+1}\right)^{\frac{1}{2}}\right) + \frac{sin\theta}{\sqrt{C}}\,x\left[tan^{-1}\left(\frac{ab - (b^2-1)sin\theta}{\sqrt{b^2-1}\sqrt{C}}\right) + tan^{-1}\left(\frac{(b^2-1)^{\frac{1}{2}}sin\theta}{\sqrt{C}}\right)\right]$$

Where,

a is the ratio of the Flame Height to Flame Radius (H/R)
b is the ratio of the distance between the center of the flame cylinder to the target to the flame radius
A is given by the equation $A = a^2 + (b+1)^2 - 2a(b+1)sin\theta$
B is given by the equation $B = a^2 + (b+1)^2 - 2a(b-1)sin\theta$

C is given by the equation $C = 1 + (b^2 + 1)cos\theta$

Atmospheric absorption

The radiation from the fire to surrounding objects will be partially attenuated by absorption and scattering along the intervening path. The principal constituents of the atmosphere that absorb thermal radiation are water vapor (H2O) and carbon dioxide (CO2) [13]. The atmospheric transmissivity is given by

$$\tau = 1 - \alpha_w - \alpha_c$$

Where the carbon dioxide vapor absorption coefficient is,

$$\alpha_c = \varepsilon_c \left(\frac{T_a}{T_s}\right)^{0.65}$$

The partial pressure of CO2 remains relatively constant at about $3x10^{-4}$ atm. The emissivity of the carbon dioxide band is shown in Figure 9 [13].

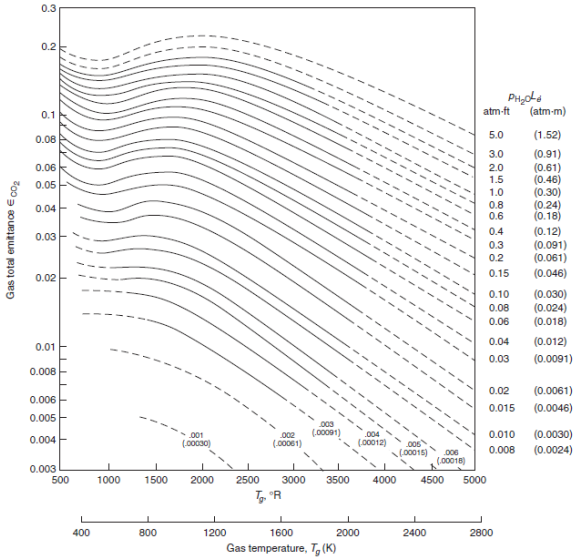

Figure 9: Total emissivity of carbon dioxide in a mixture of total pressure of 1 atm [2]

And the water vapor absorption coefficient is

$$\alpha_w = \varepsilon_w \left(\frac{T_a}{T_s}\right)^{0.45}$$

Where ε_w is determined by the partial pressure of water vapor,

$$p'_w = \frac{RH}{100} e^{\left(14.4114 - \frac{46'28}{T_a}\right)}$$

And the pathlength from the flame surface to the target is

$$p_w L = p'_w L \left(\frac{T_s}{T_a}\right)$$

The source temperature, and $p_w L$, determine the water vapor emissivity, ε_w, using emissivity plots given in Figure 10.

Lastly, the surface temperature can be determined using the

$$T_{surface} = \int_{d=1}^{120} \sqrt[4]{\left(T_{plume}^4 - \frac{\dot{q}_{plume}}{\sigma}\right)} \cos(\theta)$$

Given the atmospheric conditions for the Starlight project, assuming an annual average relative humidity of 47%, of the Starlight Project, the atmospheric transmissivity is approximately 0.918 at an elevation of 3638'.

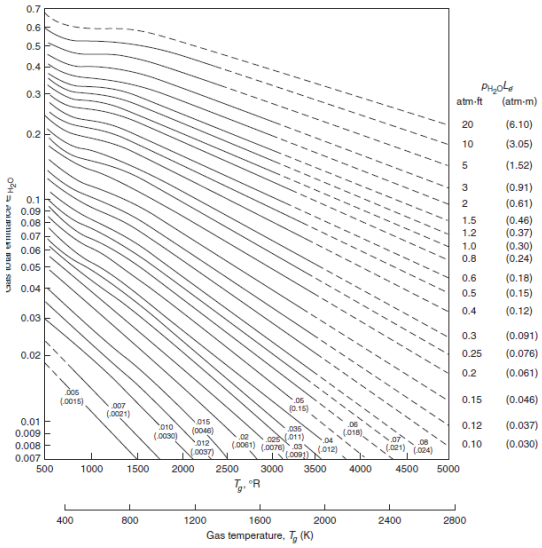

Figure 10:Total emissivity of water-vapor in a mixture of total pressure of 1 atm [13]

Wind Driven Convection Heat Transfer and Surface Level Analysis

Calculating the wind driven forced convection and the resultant contribution to the heat transfer of the surface of the adjacent ESS is subject to numerous assumptions. For the purposes of establishing bounding conditions where heat transfer is bounded and follows the work of Cengel [78].

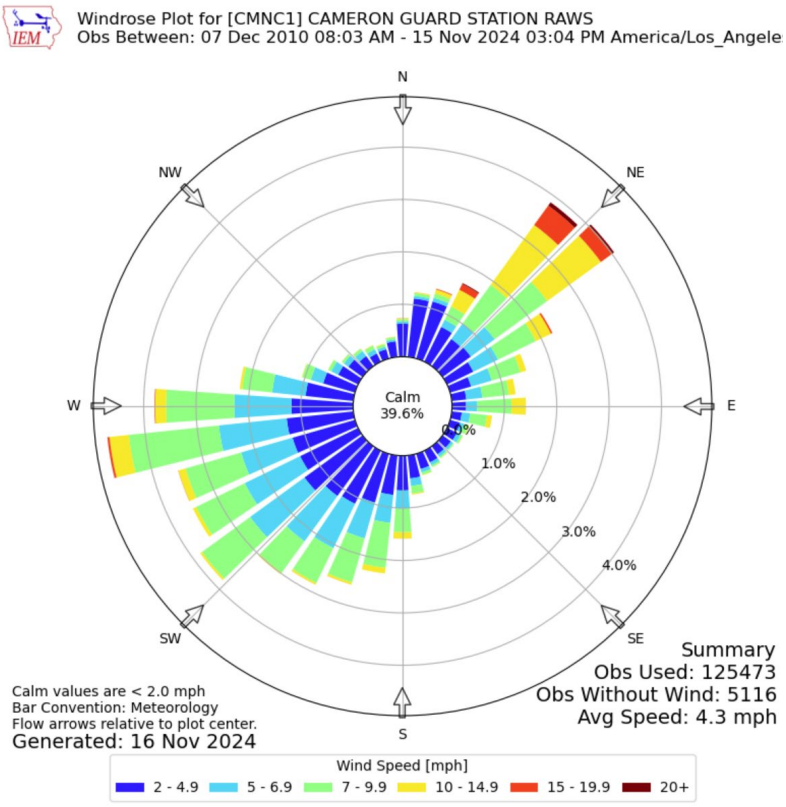

Figure 11: (ass. Typ) Cameron Guard Station Wind Rose

It is assumed a 1.92 m/s (4.3 mph) wind event over the top of an engaged structure will follow the principles in the transition from laminar to turbulent flow depending on the surface geometry, flow velocity, surface temperature, and type of fluid. For the purposes of this analysis, surface roughness is assumed to be negligible.

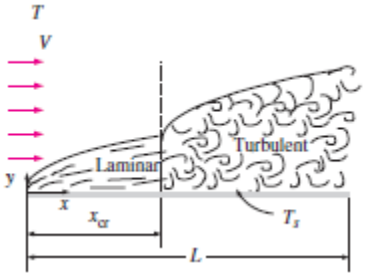

Figure 12:Analyzed Forced Convection over the top of the Engaged ESS

Assuming the top of the ESS to be a flat plate for maximum heat transfer, the Reynolds Number, the transition point where the air flow transitions from laminar to turbulent over a flat plate is governed by

$$Re_L = \frac{L\,V_L}{\nu}$$

Where L is the length of the headed surface (2.5 m, top of ESS)
V_L is the velocity of the wind event (1.92 m/s)
ν is the kinematic viscosity of air (1.338×10^{-5} m/s at 20°C) [79]

Given the Reynolds number is greater than the ideal ($5x10^5$), it is determined there is both turbulent and laminar flow over the ESS. Given the thermal conductivity of air (k = 0.02514) and the Prandtl number (P_r, 0.996 at 20°C for the City of Manzanita), the Nusselt Number (Nu) numbers for laminar assuming uniform heat flux from the surface of the ESS is

$$Nu_L = (0.664\, Re_x^{0.5}) Pr^{\frac{1}{3}}$$

The net heat flux from the top of the container assuming a heat transfer coefficient ($h = {}^{k}/_{L}\, Nu$) and applying the classical forced convection heat transfer equation [78] below

$$Q_{conv} = h\, A_s (T_1 - T_2)$$

and given the naturally occurring upward lift and wall shear of the heated air, assuming a bounding condition where 50% of the heat transfer due to convection is pulled into the passageway wake region within 10' of the container, the total heat flux to the surface of the adjacent ESS is

$$q'_{Total} = q'_{Con} + q'_{Rad}$$

The wind driven surface temperature of the adjacent ESS due to normal heat propagation, wind velocity, and direction will have an additional intermittent momentary contribution ranging from 3.9 to above 12.2 kW/m^2 within the proximity of the *ESS* containers.

Theoretical Toxic Composition of Smoke Plume

It is well documented that Lithium-ion battery fires generate intense heat and considerable amounts of gas and smoke [26, 71, 72, 80-86]. Although the emission of toxic gases can be a larger threat than heat, the knowledge of such emissions is limited for large grid-connected energy storage systems. Therefore, the following discussion outlines the findings of research into peer-reviewed publications and government sources to identify the potential toxic gas constituents in an ESS fire.

The New York State Energy Research & Development Authority (NYSERDA) and Consolidated Edison, the New York City Fire Department (FDNY) and the New York City Department of Buildings (NY DOB), commissioned DNV-GL to address code and training updates required to accommodate deployment of energy storage in New York City. The research by NYSERDA concluded "that all batteries tested emitted toxic fumes, the toxicity is similar to a plastics fire and therefore a precedent exists"[81]. Several different manufacturer battery cells were tested and the typical gases emitted included:

- Carbon monoxide (CO)
- Hydrochloride (HCI)
- Hydrogen Fluoride (HF)
- Hydrogen Cyanide (HCN)

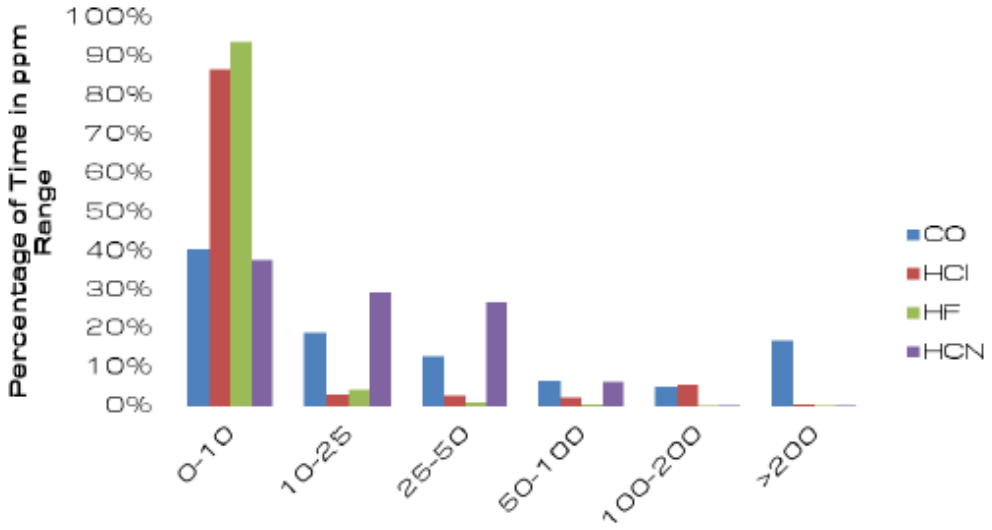

Figure 13: Representative emissions histogram from a Li-ion battery

DNV-GL concluded the "average emissions rate of a battery during a fire condition is lower per kilogram of material than a plastics fire"…."However, the peak emissions rate (during thermal runaway of a Li-ion battery, for example) is higher per kilogram of material than a plastics fire. This illustrates that a smoldering Li-ion battery on a per kilogram basis can be treated with the same precautions as something like a sofa, mattress, or office fire in terms of toxicity, but during the most intense moments of the fire (during the 2-3 minutes that cells are igniting exothermically) precautions for toxicity and ventilation should be taken. It should be noted that if Li-ion battery MODULE Modules are equipped with cascading protection, the cell failure rate may be randomized and staggered. The randomized failure rate limits the toxicity and heat release rate of the fire"[81]. However, few studies have been published that report measurements of released HF amounts from commercial Li-ion battery cells during abuse and HF release during electrolyte fire tests [82, 83, 87].

Larsson et al. studied a broad range of commercial Li-ion battery cells with different chemistry, cell design and size and included large-sized automotive-classed cells, undergoing fire tests. Their objective was to evaluate fluoride gas emissions for a large variety of battery types and for various test setups. Based on their specialized results, they determined as a function of LIB design, a wide range of amounts of HF, ranging between 20 and 200 mg/Wh of nominal battery energy capacity, were detected from the burning Li-ion batteries [82, 87, 88].

Larsson determined the vented gases can contain evaporated solvents and decomposition products, e.g. CO, CO2, H2, CH4. Besides CO, a large number of different toxic compounds can be released including fluoride gases and most concerningly Hydrogen fluoride (HF). The fluorine in the cells comes from the Li-salt, e.g. LiPF6, but also from electrode binders, e.g. PVdF, electrode materials and coatings, e.g. fluorophosphates and AlF3-coated cathodes, as well as from fluorine containing additives, e.g. flame retardants [87]. PF_5, POF_3 and HF are of greatest concern but consideration should also be given to the fluorinated phosphoric acids since they will give HF and phosphoric acid when completely reacted with water [83].

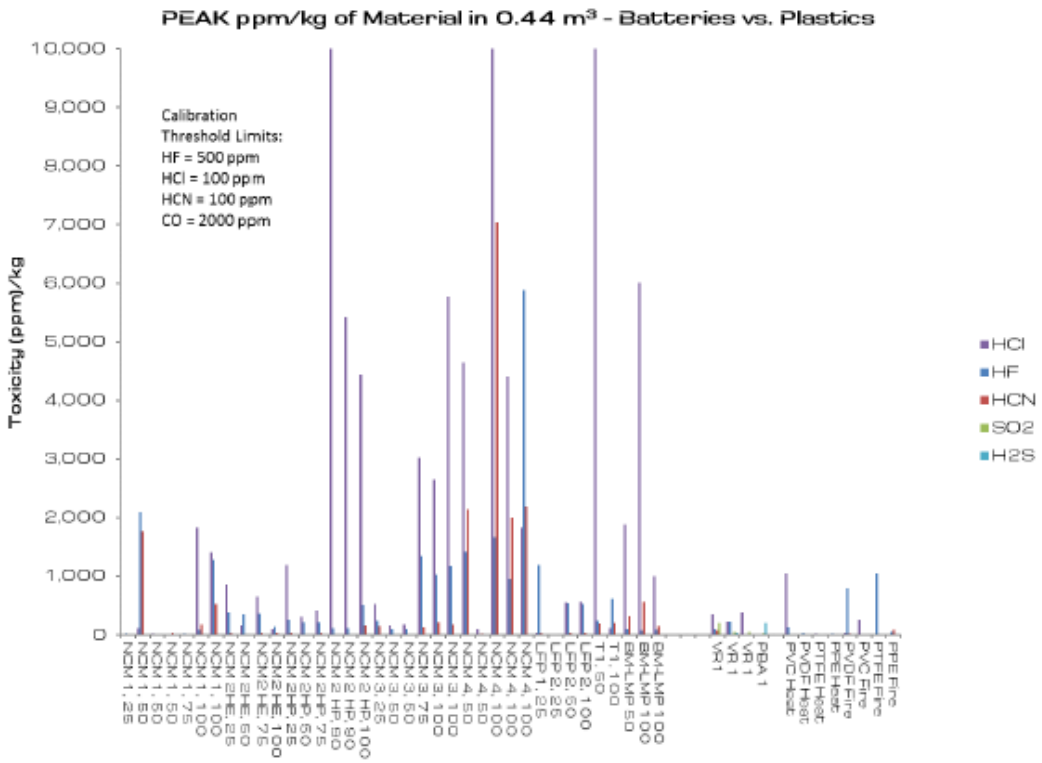

Figure 14: Peak ppm per kg (in a 0.44 m3 volume) for all batteries tested as compared to plastics [81]

The National Institute for Occupational Safety and Health (NIOSH) states that HF has a Immediately Dangerous to Life and health (IDLH) value of 30 ppm as shown in Table 2 [89]. No exposure limits are given for Phosphorus pentafluoride (PF_5) and Phosphoryl fluoride (POF_3), however their chlorine analogues, Phosphorus pentachloride (PCl_5) and Phosphoryl chloride ($POCl_3$) have recommended exposure limits (REL) values of 0.1 ppm [89].

As it pertains to the OEM LFP cells, the work performed by the SP Technical Research Institute of Sweden when testing LiFePO4, lithium ion phosphate cells, determined the measured concentrations of HF were "generally quite low but well above the detection limits" [83].

The SP Technical Research Institute of Sweden concluded based on their research "POF_3 was detected in all the small scale tests using pure electrolyte. However, no POF_3 was detected in the tests on cells. The detection limit for POF_3 was 6 ppm. Extrapolating from the small scale tests to the cells tests one ends up at concentrations below 6 ppm, which probably explains why no POF_3 was detected in these tests" [83]. "It is an important finding that POF_3 is emitted from a battery fire as this will increase the toxicity of the fire effluents. The amount of POF_3 is shown to be significant, 5-40 % of the HF emissions on a weight basis.

No PF5 could be detected in any of the tests" [83].

Table 2: NIOSH Chemical Listing for Hydrogen Fluoride (HF)

Hydrogen fluoride	**Formula:** HF	**CAS#:** 7664-39-3	**RTECS#:** MW7875000	**IDLH:** 30 ppm
Conversion: 1 ppm = 0.82 mg/m^3	**DOT:** 1052 125 (anhydrous); 1790 157 (solution)			
Synonyms/Trade Names: Anhydrous hydrogen fluoride; Aqueous hydrogen fluoride (i.e., Hydrofluoric acid); HF-A				
Exposure Limits: **NIOSH REL:** TWA 3 ppm (2.5 mg/m^3) C 6 ppm (5 mg/m^3) [15-minute] **OSHA PEL†:** TWA 3 ppm			**Measurement Methods (see Table 1):** **NIOSH** 3800, 7902, 7903, 7906 **OSHA** ID110	
Physical Description: Colorless gas or fuming liquid (below 67°F) with a strong, irritating odor. [**Note:** Shipped in cylinders.]				
Chemical & Physical Properties: **MW:** 20.0 **BP:** 67°F **Sol:** Miscible **FI.P:** NA **IP:** 15.98 eV **RGasD:** 0.69 **Sp.Gr:** 1.00 (Liquid at 67°F) **VP:** 783 mmHg **FRZ:** -118°F **UEL:** NA **LEL:** NA Nonflammable Gas	**Personal Protection/Sanitation (see Table 2):** **Skin:** Prevent skin contact (liquid) **Eyes:** Prevent eye contact (liquid) **Wash skin:** When contam (liquid) **Remove:** When wet or contam (liquid) **Change:** N.R. **Provide:** Eyewash (liquid) Quick drench (liquid)		**Respirator Recommendations (see Tables 3 and 4):** **NIOSH/OSHA** **30 ppm:** CcrS*/PaprS*/GmFS/Sa*/ScbaF **§:** ScbaF:Pd,Pp/SaF:Pd,Pp:AScba **Escape:** GmFS/ScbaE	
	Incompatibilities and Reactivities: Metals, water or steam [**Note:** Corrosive to metals. Will attack glass and concrete.]			
Exposure Routes, Symptoms, Target Organs (see Table 5): **ER:** Inh, Abs (liquid), Ing (solution), Con **SY:** Irrit eyes, skin, nose, throat; pulm edema; eye, skin burns; rhinitis; bron; bone changes **TO:** Eyes, skin, resp sys, bones		**First Aid (see Table 6):** **Eye:** Irr immed (solution/liquid) **Skin:** Water flush immed (solution/liquid) **Breath:** Resp support **Swallow:** Medical attention immed (solution)		

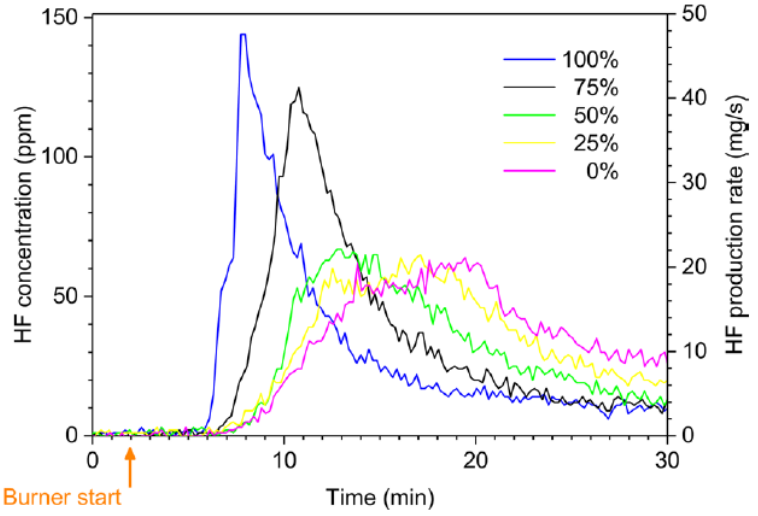

Figure 15: HF release both as the measured concentrations[82]

Lithium-Ion ESS Fire Smoke Plume Research Conclusion

Research has shown that the complex mixture of flammable and toxic gases emitted from the thermal decomposition of LIB is manufacturer and chemistry dependent. The composite breakdown of particles is a function of the size of the energy source and the inherent design chemistry that can only be estimated based on the research of others. To date, there is no readily identifiable performance data for the OEM batteries used in the *ESS* applications. Therefore, the following list of potentially flammable and toxic gases

is theoretical based on the cited works of [26, 71, 72, 80-86]:

Table 3: List of Potential Emitted Gases during Thermal Runaway

Gases Measured	Chemical Formula	Gas Type
Acetylene	C2H2	Hydrocarbons
Ethylene	C2H4	Hydrocarbons
Ethane	C2H6	Hydrocarbons
Methane	CH4	Hydrocarbons
Methanol	CH3OH	Hydrocarbons
Formaldehyde	CH2O	Hydrocarbons (Aldehydes)
Hydrogen Bromide	HBr	Hydrogen Halides
Hydrogen Chloride	HCl	Hydrogen Halides
Hydrogen Fluoride	HF	Hydrogen Halides
Hydrogen Sulfide	H2S	Sulfur Containing
Carbon Dioxide	CO2	Carbon Containing
Carbon Monoxide	CO	Carbon Containing
Ammonia	NH3	Nitrogen Containing
Hydrogen Cyanide	HCN	Nitrogen Containing
Hydrogen	H2	-
Sulfur Dioxide	SO2	Sulfur Containing

It is noted that while the DNV-GL/NYSERDA report lists only 4 emitted gases, UL testing of assumed typical LFP cell measured the following emitted gases:

Table 6 – Results of Gas Analysis			
Gas		Measured %	Component LFL
Carbon Monoxide	CO	11.191	10.9
Carbon Dioxide	CO_2	27.325	N/A
Hydrogen	H_2	48.013	4.0
Methane	CH_4	6.404	4.4
Acetylene	C_2H_2	0.107	2.3
Ethylene	C_2H_4	3.296	2.4
Ethane	C_2H_6	1.326	2.4
Propadiene (Allene)	C_3H_4	0.000	1.9
Propyne	C_3H_4	0.000	1.8
Propene	C_3H_6	0.948	1.8
Propane	C_3H_8	0.321	1.7
-	C4 (Total)	0.704	N/A
-	C5 (Total)	0.142	N/A
-	C6 (Total)	0.005	N/A
-	C7 (Total)	0.003	N/A
-	C8 (Total)	0.000	N/A
Benzene	C_6H_6	0.014	1.2
Toluene	C_7H_8	0.000	1.0
Dimethyl Carbonate	$C_3H_6O_3$	0.000	N/A
Ethyl Methyl Carbonate	$C_4H_8O_3$	0.201	N/A
Diethyl Carbonate	$C_5H_{10}O_3$	0.000	N/A
Total	-	100	-

Figure 16: EVE Vented Gas Constituents

Recommended Minimum Approach Distance

The Occupational Safety and Health Administration requires employers to establish minimum approach distance (MAD) as "the closest distance a qualified employee may approach an energized conductor or object" [90]. While directly applicable to energized circuits, the requirement of notifying employees of occupational hazards and risks and establishing both engineering and administrative controls is presented in 29CFR 1910. The Personal Protective Equipment (PPE) standard at 29 CFR 1910.132(d) requires every employer in general industry to conduct a hazard assessment to determine the appropriate PPE to be used to protect workers from the hazards identified in the assessment.

For the purposes of this analysis, the Minimum Approach Distance is defined as the closet distance a qualified employee may approach a known hazard.

While there are several different organizations (ACGIH, AIHA, OSHA, ISO, and NIOSH) that establish controls for hazard exposure, all require a job hazard analysis (JHA) be conducted to identify the hazard controls. It is assumed the appropriate JHA will be performed for each scheduled task when operating and maintaining the ESS energy storage systems.

Figure 16 depicts the maximum theoretical momentary heat flux of a potential First Responder at a distance of 3.04 m (10ft.) at an elevation of 1.5m. Table 4 presents the physiological effects of thermal radiation and the time of exposure to extreme pain and 2nd degree burns.

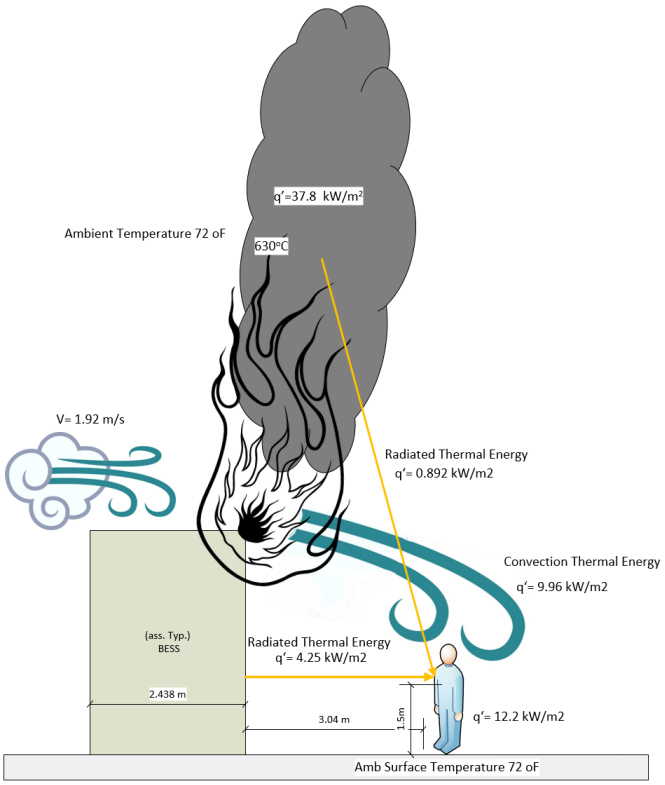

Figure 17: Maximum Theoretical Momentary Heat Flux Exposure at 3.04 m (10') at a height of 1.5m

Table 4: Physiological Effects of Thermal Radiation [91]

Time for Physiological Effects (on bare skin) to Occur Following Exposure to Specific Thermal Radiation Levels		
Radiation Intensity (kW/m2)	Time for Severe Pain (seconds)	Time for 2nd Degree Burn (seconds)
1	115	663
2	45	187
3	27	92
4	18	57
5	13	40
6	11	30
8	7	20
10	5	14
12	4	11

Figure 17 and Figure 18 present the results of an assumed comparable Plume Study results for other BESS depicting the theoretical HF dispersal as a function of distance.

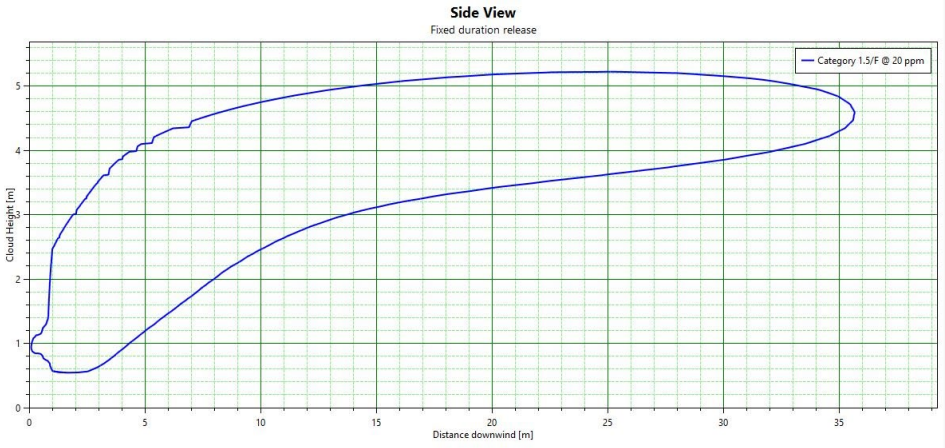

Figure 18: (typ.) 20ppm HF Cloud Dispersal Section View

Figure 19: (typ.) HF Dispersal Concentration as a Function of Distance

Therefore, assuming comparable HF generation during an engaged *ESS*, it is recommended the Minimum Approach Distances for First Responders be set at a conservative considered of a distance of 50 ft. when responding to a fire due to the potential radiated heat and potential HF exposure.

Acceptance Criteria

The Acceptance Criteria governing this NFPA 551 Fire Risk Assessment is derived from the California Fire Code where the design of the Starlight Project mitigates the probability of propagation from ESS Container to Container. Based on the information presented to Hiller, the convection and radiation heat transfer remains reasonably low. Refer to 20250320-SLS-AWp074-BOP-HMA-R0A for mitigation considerations [10].

Scenarios

From a fire protection standpoint, the overall fire hazard of any ESS is a combination of all the combustible system components, including battery chemistry, battery format (e.g., cylindrical, prismatic, polymer pouch), battery capacity and energy density, materials of construction, and component design (e.g., battery, module). To ensure confidence in the conservative approach for this FRA, the ESS are assumed to be operating under a normal operating condition, such that proprietary electronic protection systems, e.g., battery management system (BMS), are active. It is recognized that any benefit from these proprietary systems would further reduce the overall hazard, e.g., the likelihood of ignition, but it is not necessary to ensure the adequacy of protection.

The enabling assumption of the fire scenario is based on the numerous published energy storage system fires with a probability of occurrence of less than 1 %. Based the review of publicly, commercially, and internal performance data on similar LFP chemistry to the Cell and understanding the lack of propagation when heated to thermal runaway temperatures, the likelihood of a sustained fire within the *ESS* reasonably less than 1%.

Frequency and Probability Documentation

Presently, there is no adequate extinguisher solution that addresses all aforementioned fire, ignition, or flammability issues simultaneously for lithium-ion exothermic reactions. Therefore, as noted in the OEM

Energy fire protection design includes multiple extinguishers using the best available technology for mitigating a ESS fire event [71]. It is assumed, based on the evaluation of the recent global response to ESS fires, there is causality. Using the available data, it is assumed that ESS in general will experience less than a 1% failure rate resulting in fire depending on how ESS is electrically abused.

Conclusion

In this theoretical scenario, the worst case theoretical total radiant and convection heat flux on the target adjacent BESS located 10 feet across the passageway, assuming the peak wind velocity (2.2 m/s, 5 mph) based on local wind rose data will be approximately 11.14kW/m^2.

While very unlikely based on the global ESS market sector of cascading fires between adjacent containerized battery energy storage systems, if a design basis fire event is realized and is unnoticed and unmitigated, an adjacent *ESS* Thermal Management System should be able to control the internal environment but could eventually shutdown when internal temperatures exceed pre-established setpoints (typically 90°F/32 °C). Once the internal thermal management is no longer in operation, the heat transfer from the adjacent fully developed container fire could, as a function of the fire lifecycle and thermal insulation degradation, could exceed the thermal stability thresholds of the adjacent racks.

Data Sources

[1] *NFPA 855: Standard for the Installation of Stationary Energy Storage Systems*, NFPA, Quincy, MA, August 25 2023.

[2] *2021 International Fire Code*, I. IFC, Country Club Hills, IL, 3 November 2021.

[3] OSHA. "Process Safety Management." United States Departmetn of Labor, Occupational Safety and Health Administration. https://www.osha.gov/process-safety-management (accessed 9 April 2025, 2025).

[4] OSHA. "RAGAGEP in Process Safety Management Enforcement." United States Departmetn of Labor, Occupational Safety and Health Administration. https://www.osha.gov/laws-regs/standardinterpretations/2016-05-11 (accessed 9 April 2025, 2025).

[5] D. Hill, "Technical Support for APS Related to Mcmicken Thermal Runaway and Explosion: McMicken Battery Energy Storage System Event Technical Analysis and Recommendations," DNV GL Energy Insights USA, Inc., Chalfont, PA, 18 July 2020 2020.

[6] Wartsila, "Schematic Diagram of Gridsolv Quantum Duke Energy - Nebo Morganton, NC US 3.0 MW/8.64 MWh," in *P24458 Duke Energy - Nebo*, 2.0 ed. Houston TX: Wartsila, 2024, pp. 1-68.

[7] CSA, "Project 80146723: CSA Group Laboratory Test Data – UL 9540A Report and Test Result for BYD model MC-B536-U-R4M01," CCIC-CSA International Certification Co., Ltd. Kunshan Branch, Kunshan, Jiangsu China, Project 80146723, 2 April 2023.

[8] UL, "Module Test Report - UL 9540A Test Method for Evaluating Thermal Runaway Fire Propagation in Battery Energy Storage Systems (AACD)," Underwriters Laboratory, Northbrook IL, 20 January 2022.

[9] UL, "Cell Test Report - UL 9540A Test Method for Evaluating Thermal Runaway Fire Propagation in Battery Energy Storage Systems (AACD)," Underwriters Laboratory, Northbrook IL, 14 October 2020.

[10] R. Steele, "Empire II LLC Starlight Project Balance of Hazard Mitigation Analysis," Hiller, Wilmington NC, 25 April 2025.

[11] NFPA, "NFPA 551: guide for the evaluation of fire risk assessments," *National Fire Protection Association, Quincy, USA,* 2016.

[12] *Engineering Guide: Fire Risk Assessment*, SFPE, Gaithersburg, MD, 2006.

[13] M. J. Hurley *et al.*, *SFPE Handbook of Fire Protection Engineering*. Quincy, Massachusetts: National Fire Protection Association, 2015.

[14] *ISO 16732-1: Fire Safety Engineering - Fire RIsk Assessment, Part 1 - General*, ISO, Geneva, Switzerland, 15 February 2012 2012.

[15] *ISO 16732-1: Fire Safety Engineering - Fire RIsk Assessment, Part 3: Example of an Industrial Property*, ISO, Geneva, Switzerland, 15 February 2012 2012.

[16] DOE, "Battery Storage in the United States: An Update on Market Trends," ed. Washington DC: US Department of Energy, US Energy Information Administration 2021.

[17] DOE. "Renewable Electricity Infrastructure and Resources Dashboard." US Department of Energy, US Energy Information Administration https://eia.maps.arcgis.com/apps/dashboards/77cde239acfb494b81a00e927574e430 (accessed.

[18] S. Xue, C. Chen, Y. Jin, Y. Li, B. Li, and Y. Wang, "Protection for DC distribution system with distributed generator," *Journal of Applied Mathematics,* vol. 2014, 2014.

[19] F. Xu *et al.*, "Failure investigation of LiFePO4 cells under overcharge conditions," *Journal of The Electrochemical Society,* vol. 159, no. 5, p. A678, 2012.

[20] Z. Xing, J. Mao, Y. Huang, J. Zhou, W. Mao, and F. Deng, "Scaled experimental study on

maximum smoke temperature along corridors subject to room fires," *Sustainability,* vol. 7, no. 8, pp. 11190-11212, 2015.

[21] Q. Wang, P. Ping, X. Zhao, G. Chu, J. Sun, and C. Chen, "Thermal runaway caused fire and explosion of lithium ion battery," *Journal of power sources,* vol. 208, pp. 210-224, 2012.

[22] Q. Wang, B. Mao, S. I. Stoliarov, and J. Sun, "A review of lithium ion battery failure mechanisms and fire prevention strategies," *Progress in Energy and Combustion Science,* vol. 73, pp. 95-131, 2019.

[23] J. Vetter *et al.*, "Ageing mechanisms in lithium-ion batteries," *Journal of power sources,* vol. 147, no. 1-2, pp. 269-281, 2005.

[24] G. Pistoia, *Lithium-ion batteries: advances and applications*. Newnes, 2013.

[25] P. Ping *et al.*, "Study of the fire behavior of high-energy lithium-ion batteries with full-scale burning test," *Journal of Power Sources,* vol. 285, pp. 80-89, 2015.

[26] D. Ouyang, M. Chen, Q. Huang, J. Weng, Z. Wang, and J. Wang, "A review on the thermal hazards of the lithium-ion battery and the corresponding countermeasures," *Applied Sciences,* vol. 9, no. 12, p. 2483, 2019.

[27] B. Ditch and D. Zeng, "Research Technical Report: Development of Sprinkler Protection Guidance for Lithium Ion Based Energy Storage Systems," FM Global, Norwood, MA, June 2019 2019.

[28] NFPA, "Sprinkler Protection Guidance for Lithium-Ion Based Energy Storage Systems," National Fire Protection Association, Quincy, MA USA, June 2019 2019. [Online]. Available: https://www.nfpa.org//-/media/Files/News-and-Research/Fire-statistics-and-reports/Suppression/RFESSSprinklerProtection.pdf

[29] A. E. Cote, *NFPA No.: FPH2008 - Fire Protection Handbook*, Twentieth Edition ed. Quincy, MA: National Fire Protection Assoc, 2008.

[30] CSA, "Project 80040846: CSA Group hereby confirms that it has completed an evaluation of: Li-ion Battery Cell, models 001CB310, CB310 and CB2W0," CSA Group, Ningde City, China, Project 80040846, 22 July 2020.

[31] *NFPA 855: Standard for the Installation of Stationary Energy Storage Systems*, NFPA, Quincy, MA, August 25, 2019 2020.

[32] ABM. *Industrial Insulation* (2021). Shanghai, China: Shanghai ABM Rock Wool Co, Ltd. .

[33] F. Larsson and B.-E. Mellander, "Abuse by external heating, overcharge and short circuiting of commercial lithium-ion battery cells," *Journal of The Electrochemical Society,* vol. 161, no. 10, p. A1611, 2014.

[34] X. Meng *et al.*, "Internal failure of anode materials for lithium batteries—A critical review," *Green Energy & Environment,* vol. 5, no. 1, pp. 22-36, 2020.

[35] A. W. Golubkov *et al.*, "Thermal runaway of commercial 18650 Li-ion batteries with LFP and NCA cathodes–impact of state of charge and overcharge," *Rsc Advances,* vol. 5, no. 70, pp. 57171-57186, 2015.

[36] A. W. Golubkov *et al.*, "Thermal-runaway experiments on consumer Li-ion batteries with metal-oxide and olivin-type cathodes," *Rsc Advances,* vol. 4, no. 7, pp. 3633-3642, 2014.

[37] P. J. Bugryniec, J. N. Davidson, D. J. Cumming, and S. F. Brown, "Pursuing safer batteries: thermal abuse of LiFePO4 cells," *Journal of Power Sources,* vol. 414, pp. 557-568, 21 January 2019 2019.

[38] N. Gao *et al.*, "Fast diagnosis of failure mechanisms and lifetime prediction of Li metal batteries," *Small Methods,* vol. 5, no. 2, p. 2000807, 2021.

[39] W. Tang, W. C. Tam, L. Yuan, T. Dubaniewicz, R. Thomas, and J. Soles, "Estimation of the critical external heat leading to the failure of lithium-ion batteries," *Applied thermal engineering,* vol. 179, p. 115665, 2020.

[40] A. Sarkar, I. C. Nlebedim, and P. Shrotriya, "Performance degradation due to anodic failure mechanisms in lithium-ion batteries," *Journal of Power Sources,* vol. 502, p. 229145, 2021.

[41] R. T. L. Jr., J. A. Sutula, and M. J. Kahn, "Lithium Ion Batteries Hazard and Use Assessment Phase IIB, Flammability Characterization of Li-ion Batteries for Storage Protection," The Fire Protection Research Foundation, Quincy MA, April 29, 2013 2013.

[42] N. Williard, W. He, C. Hendricks, and M. Pecht, "Lessons learned from the 787 Dreamliner issue on lithium-ion battery reliability," *Energies,* vol. 6, no. 9, pp. 4682-4695, 2013.

[43] S. Koch, K. Birke, and R. Kuhn, "Fast thermal runaway detection for lithium-ion cells in large scale traction batteries," *Batteries,* vol. 4, no. 2, p. 16, 27 March 2018 2018. [Online]. Available: www.mdpi.com/journal/batteries.

[44] T. Ohsaki *et al.*, "Overcharge reaction of lithium-ion batteries," *Journal of Power Sources,* vol. 146, no. 1-2, pp. 97-100, 2005.

[45] B. Ditch and C. Wieczorek, "Flammability characterization of Li-ion batteries in bulk storage," Technical Report, FM Global, 2013, available at www. fmglobal. com …, 2013.

[46] D. Belov and M.-H. Yang, "Failure mechanism of Li-ion battery at overcharge conditions," *Journal of Solid State Electrochemistry,* vol. 12, no. 7-8, pp. 885-894, 2008. [Online]. Available: https://www.researchgate.net/profile/Dmitry_Belov6/publication/226507209_Failure_mechanism_of_Li-ion_battery_at_overcharge_conditions/links/56fb42cb08ae8239f6dadb98.pdf.

[47] Celina Mikolajczak, Michael Kahn, Kevin White, and Richard Thomas Long, "Lithium-Ion Batteries Hazard and Use Assessment - Final Report," The Fire Protection Research Foundation, Quincy MA, July 2011 2011.

[48] S. Cummings. "South Korea Identifies Top 4 Causes that Led to ESS Fires." Li-ion Tamer. https://liiontamer.com/south-korea-identifies-top-4-causes-that-led-to-ess-fires/ (accessed 26 July 2019, 2019).

[49] N. Ponchaut, K. Marr, F. Colella, V. Somandepalli, and Q. Horn, "Thermal runaway and safety of large lithium-ion battery systems," *Proceedings of the The Battcon,* pp. 17.1-17.10, 2015.

[50] J. Lamb, C. J. Orendorff, L. A. M. Steele, and S. W. Spangler, "Failure propagation in multi-cell lithium ion batteries," *Journal of Power Sources,* vol. 283, pp. 517-523, 2015.

[51] "IEEE Standard for Rechargeable Batteries for Multi-Cell Mobile Computing Devices," *IEEE Std 1625-2008 (Revision of IEEE Std 1625-2004),* pp. c1-79, 2008, doi: 10.1109/IEEESTD.2008.4657368.

[52] DNV-GL, "McMicken Battery Energy Storage System Event Technical Analysis and Recommendations," Chalfont, PA, 18 July 2020 2020.

[53] *ANSI/CAN/UL-1973:2018, Batteries for Use in Stationary, Vehicle Auxiliary Power and Light Electric Rail (LER) Applications*, UL, Northbrook, IL, February 7, 2018 2018.

[54] NHTSA, "Lithium-ion Battery Safety Issues for Electric and Plug-in Hybrid Vehicles," US Department of Transportation, National Highway Traffic Safety Administration, Washington D.C., October 2017 2017. [Online]. Available: https://www.nhtsa.gov/sites/nhtsa.dot.gov/files/documents/12848-lithiumionsafetyhybrids_101217-v3-tag.pdf

[55] UL, "Module Test Report UL 9540A Test Method for Evaluating Thermal Runaway Fire Propagation in Battery Energy Storage Systems (AACD) [Samsung SDI MS8943E101A]," Underwriters Laboratory, GYEONGGI-DO, Republic of Korea, 4789768841, 25 May 2022.

[56] M. Ghiji *et al.*, "A Review of Lithium-Ion Battery Fire Suppression," *Energies,* vol. 13, no. 19, p. 5117, 2020.

[57] X. Hu, K. Zhang, K. Liu, X. Lin, S. Dey, and S. Onori, "Advanced fault diagnosis for lithium-ion

battery systems: A review of fault mechanisms, fault features, and diagnosis procedures," *IEEE Industrial Electronics Magazine,* vol. 14, no. 3, pp. 65-91, 2020.

[58] S. Mallick and D. Gayen, "Thermal behaviour and thermal runaway propagation in lithium-ion battery systems–A critical review," *Journal of Energy Storage,* vol. 62, p. 106894, 2023.

[59] L. Kong, C. Li, J. Jiang, and M. Pecht, "Li-ion battery fire hazards and safety strategies," *Energies,* vol. 11, no. 9, p. 2191, 2018.

[60] S. Wang, Z. Du, Z. Han, Z. Zhang, L. Liu, and J. Hao, "Study of the Temperature and Flame Characteristics of Two Capacity LiFePO4 Batteries in Thermal Runaway," *Journal of The Electrochemical Society,* vol. 165, no. 16, pp. A3828-A3836, 2018, doi: 10.1149/2.0531816jes.

[61] A. Blum and R. Long Jr, "Lithiu m Ion Batteries Hazard and Use Assessment - Phase III," in "Fire Protection Research Foundation," Fire Protection Research Foundation, Quincy, MA, November 2016 2016.

[62] A. F. Blum and R. T. Long Jr, *Fire Hazard Assessment of Lithium Ion Battery Energy Storage Systems*. Springer Nature, 2016.

[63] ACORE. "U.S. Energy Storage Market Primed for Growth." American Council on Renewable Energy. https://acore.org/resources/u-s-energy-storage-market-primed-for-growth/ (accessed 9 April, 2024).

[64] DNV-GL, "Safety, Operation and Performance of Grid Connected Energy Storage Systems," vol. DNVGL-RP-0043, ed. Oslo, Norway: Det Norske Veritas Holding AS, 2017.

[65] S. J. Harris, D. J. Harris, and C. Li, "Failure statistics for commercial lithium ion batteries: A study of 24 pouch cells," *Journal of Power Sources,* vol. 342, pp. 589-597, 2017.

[66] J. Quintiere, *Fundamentals of fire phenomena*. Wiley, 2006.

[67] CSA, "Project 80040846: CSA Group Laboratory Test Data – UL 9540A Report and Test Result for Contemporary Amperex Technology Co., Limited," CSA Group, Fujian Province 352100, P. R. China, Project 80016523, 22 July 2020.

[68] V. Hutchinson, "Li-Ion Battery Energy Storage Systems: Effect of Separation Distances based on a Radiation Heat Transfer Analysis," Worcester Polytechnic Institute, Worcester, MA, 12 June 2017.

[69] UL, "Cell Test Report: UL 9540A Test Method for Evaluating Thermal Runaway Fire Propagation in Battery Energy Storage Systems (AACD)," Underwriters Laboratory, LLC, Jingmen, CN, 30 April 2021.

[70] F. Larsson, P. Andersson, P. Blomqvist, and B.-E. Mellander, "Toxic fluoride gas emissions from lithium-ion battery fires," *Scientific reports,* vol. 7, no. 1, pp. 1-13, 2017.

[71] DNV-GL, "Testing of Aerosol Fire Extinguishing Agent for Li-ion Battery Fires," vol. 10030271 – HOU – R -01, ed. Rochester, NY: Det Norske Veritas (DNV) GL - Energy Advisory Americas, 2017.

[72] J. Lamb, C. J. Orendorff, E. P. Roth, and J. Langendorf, "Studies on the thermal breakdown of common Li-ion battery electrolyte components," *Journal of The Electrochemical Society,* vol. 162, no. 10, pp. A2131-A2135, 2015.

[73] A. Blum and R. Long Jr, "Hazard assessment of lithium ion battery energy storage systems," in "Fire Protection Research Foundation," Fire Protection Research Foundation, Bowie, MD, February 2016 2016.

[74] D. Pitts and L. Sissom, *Schaum's Outline of Theory and Problems of Heat Transfer* 2ed. (Schaum's Outline Series). New York, NY: McGraw Hill, 1988.

[75] D. Drysdale, *An introduction to fire dynamics*. John Wiley & Sons, 2011.

[76] J. Pokorný, "Determination of centreline temperature of Fire Plume with respect to a gas hot layer," presented at the Fire Engineernig, 3nd International Scientific Conference,

Technical university in Zvolen, Slovak republic, January 2010, 2010. [Online]. Available: https://www.researchgate.net/publication/269990367_Determination_of_centreline_temperature_of_Fire_Plume_with_respect_to_a_gas_hot_layer.

[77] U. Wickström, D. Duthinh, and K. B. McGrattan, "Adiabatic surface temperature for calculating heat transfer to fire exposed structures," in *Proceedings of the Eleventh International Interflam Conference. Interscience Communications, London*, 2007, vol. 167.

[78] Y. Cengel, *Heat and mass transfer: fundamentals and applications*. McGraw-Hill Higher Education, 2014.

[79] "Viscosity of Air, Dynamic and Kinematic." Engineers Edge, LLC. https://www.engineersedge.com/physics/viscosity_of_air_dynamic_and_kinematic_14483.htm (accessed 17 February 2020.

[80] A. Nedjalkov *et al.*, "Toxic gas emissions from damaged lithium ion batteries—analysis and safety enhancement solution," *Batteries,* vol. 2, no. 1, p. 5, 2016.

[81] DNV-GL, "Considerations for ESS Fire Safety," 3rd ed. Dublin, OH: Det Norske Veritas (U.S.A.), Inc. (DNV GL), 2017.

[82] F. Larsson, P. Andersson, P. Blomqvist, and B.-E. Mellander, "Toxic fluoride gas emissions from lithium-ion battery fires," *Scientific reports,* vol. 7, no. 1, p. 10018, 2017.

[83] P. Andersson, P. Blomqvist, A. Loren, and F. Larsson, *Investigation of fire emissions from Li-ion batteries*. 2013.

[84] P. Ribière, S. Grugeon, M. Morcrette, S. Boyanov, S. Laruelle, and G. Marlair, "Investigation on the fire-induced hazards of Li-ion battery cells by fire calorimetry," *Energy & Environmental Science,* vol. 5, no. 1, pp. 5271-5280, 2012.

[85] A. Lecocq, G. G. Eshetu, S. Grugeon, N. Martin, S. Laruelle, and G. Marlair, "Scenario-based prediction of Li-ion batteries fire-induced toxicity," *Journal of Power Sources,* vol. 316, pp. 197-206, 2016.

[86] N. S. Spinner *et al.*, "Physical and chemical analysis of lithium-ion battery cell-to-cell failure events inside custom fire chamber," *Journal of Power Sources,* vol. 279, pp. 713-721, 2015.

[87] F. Larsson, S. Bertilsson, M. Furlani, I. Albinsson, and B.-E. Mellander, "Gas explosions and thermal runaways during external heating abuse of commercial lithium-ion graphite-LiCoO2 cells at different levels of ageing," *Journal of power sources,* vol. 373, pp. 220-231, 2018.

[88] F. Larsson, P. Andersson, P. Blomqvist, A. Lorén, and B.-E. Mellander, "Characteristics of lithium-ion batteries during fire tests," *Journal of Power Sources,* vol. 271, pp. 414-420, 2014.

[89] M. E. Barsan, "NIOSH pocket guide to chemical hazards," 2007.

[90] (2021). *1926.968 - Definitions*. [Online] Available: https://www.osha.gov/laws-regs/regulations/standardnumber/1926/1926.968

[91] F. E. M. Agency, "Handbook of Chemical Hazard Analysis Procedures," ed: US EPAU. S. DOT, 1993.